

The PAMELA excess from neutralino annihilation in the NMSSM

Yang Bai^a, Marcela Carena^{a,b} and Joseph Lykken^a

^a*Fermi National Accelerator Laboratory, P.O. Box 500, Batavia, IL 60510, USA*

^b*Enrico Fermi Institute, Univ. of Chicago, 5640 Ellis Ave., Chicago, IL 60637, USA*

Abstract

The cosmic ray positron excess observed by PAMELA can be explained by neutralino annihilation in the Next-to-Minimal Supersymmetric Standard Model (NMSSM). The main dark matter annihilation products are the lightest CP -even scalar h_1 plus the lightest CP -odd scalar a_1 , with the a_1 decaying into two muons. The energetic positrons needed to explain PAMELA are thus obtained in the NMSSM simply from kinematics. The required large annihilation cross section is obtained from an s -channel resonance with the heavier CP -odd scalar a_2 . Various experiments constrain the PAMELA-favored NMSSM parameter space, including collider searches for a light a_1 . These constraints point to a unique corner of the NMSSM parameter space, having a lightest neutralino mass around 160 GeV and a very light pseudoscalar mass less than a GeV. A simple parameterized formula for the charge-dependent solar modulation effects reconciles the discrepancy between the PAMELA data and the estimated background at lower energies. We also discuss the electron and gamma ray spectra from the Fermi LAT observations. An NMSSM explanation of PAMELA makes three striking and uniquely correlated predictions: the rise in the PAMELA positron spectrum will turn over at around 70 GeV, the dark matter particle mass is less than the top quark mass, and a light sub-GeV pseudoscalar will be discovered at colliders.

1 Introduction

Recently, the PAMELA collaboration has observed an anomalous positron abundance in cosmic radiation [1]. The positron over electron fraction turns over and appears to rise at energies from 10 GeV to 100 GeV. However, from the same detector, no obvious antiproton excess is seen for the same energy range [2]. Many suggestions have been made to explain the positron excess at PAMELA. Among different approaches, dark matter annihilation is especially interesting and could imply future signals in dark matter direct detection experiments and/or at the Large Hadron Collider (LHC).

In recent model-independent studies, dark matter particles are required both to annihilate dominantly to leptons and to have a much larger annihilation rate in the galactic halo than would be implied by a traditional thermal relic estimate [3] [4]. The lack of antiproton excess in the PAMELA experiment [2] can be explained if dark matter particles first annihilate into some intermediate particles, which are so light that their decays to hadrons are kinematically forbidden [5], or couple dominantly to Standard Model (SM) leptons [6]. To explain the large dark matter annihilation cross section in the galactic halo while remaining consistent with a thermal dark matter relic abundance, one can introduce an attractive force between two dark matter particles and use the Sommerfeld enhancement to boost the annihilation cross section in the galactic halo [7]. This scenario suggests interesting signatures [8] and can be tested at the LHC [9]. A second approach is to consider non-thermal relics. Other long-lived particles can decay to the dark matter particles and increase the dark matter relic abundance in the galactic halo [10].

Instead of constructing a dark matter model *ad hoc* to explain the cosmic ray observations, in this paper we ask whether there is an existing well-motivated model that naturally contains the necessary ingredients to explain the positron excess of PAMELA. The most developed framework to address the naturalness problem of the SM is the Minimal Supersymmetric Standard Model (MSSM), which provides the lightest superpartner (LSP) protected by R-parity as the dark matter candidate. In general, the annihilation products in the MSSM contain not only leptons but also a large fraction of hadrons. This makes it

difficult for the MSSM to explain the positron excess at PAMELA, and at the same time be consistent with the antiproton spectrum at PAMELA [11]. From the theoretic side, the MSSM suffers the μ -problem, which can be solved elegantly by introducing a new gauge singlet chiral supermultiplet, as proposed in the Next-to-Minimal Supersymmetric Standard Model [12]. A recent exploration of the NMSSM parameter space shows that the lightest CP -odd particle a_1 (mainly from the singlet component) can be naturally lighter than $2m_b$ and mainly decay into two τ 's [13]. One should notice that the mass of a_1 in the NMSSM is protected by the $U(1)_R$ symmetry and can even be lighter than 1 GeV if the soft terms associated with the singlet are small. In this case the a_1 will decay mainly into two muons for a mass of a few hundred MeV.

Therefore, if the dark matter candidate in the NMSSM can annihilate mostly into a_1 's, we can have a leptonic final state in the annihilation products simply from kinematics. The NMSSM provides the necessary ingredients to make this happen. Notice that the dark matter candidate in the NMSSM is the LSP neutralino (for existing studies for light neutralino dark matter in the NMSSM, see [14]). If its mass happens to be around half that of the heavier CP -odd scalar a_2 mass, a large dark matter annihilation cross section is obtained through the s -channel resonance effects with a_2 . To have leptons dominant in the final state, we should have a large branching ratio of a_2 to a_1 plus h_1 . This will naturally happen, provided that the dark matter LSP mass is less than the top quark mass, and thus that the decay of a_2 to $t\bar{t}$ is kinematically forbidden. Since the CP -odd scalar coupling to other fermions is proportional to their Yukawa couplings, the final state can dominantly be $a_1 + h_1$ with the former decaying to leptons. The kinematics helps us to obtain hard leptons in the final state of the dark matter annihilations.

In Section 2, we develop the notation by deriving the spectrum and interactions in the NMSSM, and show two sets of representative model points allowed by current experimental constraints. We calculate the dark matter annihilation cross section in Section 3 and positron excesses from neutralino annihilation in Section 4. In Section 5, we consider the constraints on the model parameter space from the PAMELA antiproton spectrum. We discuss the gamma-ray spectrum in Section 6 and also make predictions for Fermi LAT. In Section 7 we

demonstrate the consistency of our model points with direct constraints from LEP, Tevatron, CLEO, B-factories and the magnetic moment of the muon. Finally, we discuss dark matter direct detection and conclude in Section 8.

2 Spectrum and interactions in the NMSSM

To describe the NMSSM model, we follow the notation in the Ref. [15]. The superpotential in the NMSSM is

$$W = \lambda \hat{S} \hat{H}_u \hat{H}_d + \frac{\kappa}{3} \hat{S}^3, \quad (1)$$

and the soft supersymmetry-breaking terms are

$$V = \lambda A_\lambda S H_u H_d + \frac{\kappa}{3} A_\kappa S^3 + h.c.. \quad (2)$$

Here, hatted capital letters denote superfields, and unhatted capital letters the corresponding scalar components. The minimization of the scalar potential determines their vacuum expectation values (VEVs): $h_u \equiv \langle H_u \rangle$, $h_d \equiv \langle H_d \rangle$ and $s \equiv \langle S \rangle$. The electroweak scale $v = \sqrt{h_u^2 + h_d^2} = 174$ GeV. Since $\mu_{\text{eff}} = \lambda s$, there are four new parameters in the NMSSM, which we take to be real: λ , A_λ , κ and A_κ . With sign conventions for the fields, λ and $\tan \beta \equiv h_u/h_d$ are positive, while A_λ , κ , A_κ and μ_{eff} can have either sign.

There exists a \mathcal{Z}_3 symmetry for the NMSSM, which is spontaneously broken and induces a domain wall problem. One can introduce higher dimension operators to explicitly break this discrete symmetry and perhaps circumvent this problem [16]. Since those \mathcal{Z}_3 breaking operators have small effects on the analysis performed in this paper, we will neglect them from now on.

2.1 Neutralinos

There are five neutralinos in the NMSSM: the $U(1)_Y$ gaugino λ_1 , the neutral $SU(2)_W$ gaugino λ_2 , the Higgsinos ψ_u^0 and ψ_d^0 and the singlino ψ_s . In the basis $\psi^0 = (-i\lambda_1, -i\lambda_2, \psi_u^0, \psi_d^0, \psi_s)$,

we have the neutralino mass matrix

$$\mathcal{L} = -\frac{1}{2} (\psi^0)^T \mathcal{M}_0 (\psi^0) + h.c., \quad (3)$$

where

$$\mathcal{M}_0 = \begin{pmatrix} M_1 & 0 & \frac{g_1 h_u}{\sqrt{2}} & -\frac{g_1 h_d}{\sqrt{2}} & 0 \\ 0 & M_2 & -\frac{g_2 h_u}{\sqrt{2}} & \frac{g_2 h_d}{\sqrt{2}} & 0 \\ \frac{g_1 h_u}{\sqrt{2}} & -\frac{g_2 h_u}{\sqrt{2}} & 0 & -\mu & -\lambda h_d \\ -\frac{g_1 h_d}{\sqrt{2}} & \frac{g_2 h_d}{\sqrt{2}} & -\mu & 0 & -\lambda h_u \\ 0 & 0 & -\lambda h_d & -\lambda h_u & 2\kappa s \end{pmatrix}. \quad (4)$$

To obtain the needed dark matter annihilation rate, we consider the case that the LSP, the lightest neutralino, is mainly made of the bino with mixings with Higgsinos. For $g_i v, \lambda v \ll |M_1| < |\mu| < |M_2|$, a moderate $\tan \beta > 1$ and $\mu < 0$, the lightest neutralino is approximately

$$\chi \approx -i\lambda_1 - (\sin \alpha_1 \cos \beta - \sin \alpha_2 \sin \beta) \psi_u^0 - (\sin \alpha_2 \cos \beta + \sin \alpha_1 \sin \beta) \psi_d^0, \quad (5)$$

with

$$\alpha_1 = \frac{1}{2} \arctan \frac{\sqrt{2} g_1 v \mu \cos 2\beta}{\mu^2 - M_1^2 + (\lambda^2 - g_1^2/2)v^2}, \quad (6)$$

$$\alpha_2 = \frac{1}{2} \arctan \frac{\sqrt{2} g_1 v (M_1 + \mu \sin 2\beta)}{M_1^2 - \mu^2}, \quad (7)$$

and with its mass approximated as

$$m_\chi = M_1 + \frac{g_1^2 v^2 (M_1 + \mu \sin 2\beta)}{2(M_1^2 - \mu^2)}. \quad (8)$$

Hereafter, we use a simple notation χ to replace the usual notation $\tilde{\chi}_1^0$ for the lightest neutralino.

2.2 Higgs sector at tree level

The charged Higgs $H^\pm = \cos \beta H_u^\pm + \sin \beta H_d^\pm$ has a mass

$$M_{H^\pm}^2 = \lambda s (A_\lambda + \kappa s) \frac{2}{\sin 2\beta} + \left(\frac{g_2^2}{2} - \lambda^2\right) v^2. \quad (9)$$

For κ and λ of order of unity, the mass of H^\pm is generically $\mathcal{O}(\mu)$.

Expanding around the Higgs fields VEVs, the neutral scalar fields are defined as

$$H_u^0 = h_u + \frac{H_{uR} + i H_{uI}}{\sqrt{2}}, \quad H_d^0 = h_d + \frac{H_{dR} + i H_{dI}}{\sqrt{2}}, \quad S = s + \frac{S_R + i S_I}{\sqrt{2}}. \quad (10)$$

For the three CP -even neutral states, we can diagonalize their 3×3 mass matrix by an orthogonal matrix S_{ij} to obtain the mass eigenstates (ordered in mass): $h_i = S_{ij} (H_{uR}, H_{dR}, S_R)_j$, with masses denoted by m_{h_i} . For $v \ll s$, we write the lightest CP -even Higgs as

$$h_1 \approx \cos \alpha \cos \theta_S H_{uR} + \sin \alpha \cos \theta_S H_{dR} - \sin \theta_S S_R, \quad (11)$$

with

$$\begin{aligned} \alpha &\approx \frac{\pi}{2} - \beta - \frac{\lambda M_Z^2 \sin 2\beta \sin 4\beta}{4 \kappa \mu^2}, \\ \theta_S &= -\frac{\lambda^2 v}{2 \kappa^2 s} \left(1 - \frac{\kappa}{\lambda} \sin 2\beta\right) + \mathcal{O}(v^3/s^3). \end{aligned} \quad (12)$$

The singlet component of h_1 is small and suppressed by v/s .

There are three CP -odd pseudoscalar fields, one of which is a massless Goldstone mode eaten by the Z boson. Dropping the Goldstone mode, the remaining 2×2 mass matrix in the (\tilde{A}, S_I) basis with $\tilde{A} \equiv \cos \beta H_{uI} + \sin \beta H_{dI}$, is

$$\mathcal{M}_{\text{odd}} = \begin{pmatrix} \lambda s \frac{h_u^2 + h_d^2}{h_u h_d} (A_\lambda + \kappa s) & \lambda \sqrt{h_u^2 + h_d^2} (A_\lambda - 2 \kappa s) \\ \lambda \sqrt{h_u^2 + h_d^2} (A_\lambda - 2 \kappa s) & 4 \lambda \kappa h_u h_d + \lambda A_\lambda \frac{h_u h_d}{s} - 3 \kappa A_\kappa s \end{pmatrix}. \quad (13)$$

We introduce a mixing angle θ_A to diagonalize the above matrix:

$$\tan \theta_A = -\frac{2 s (A_\lambda + \kappa s)}{v (A_\lambda - 2 \kappa s) \sin 2\beta}, \quad (14)$$

$$\cos^2 \theta_A = \frac{v^2 (A_\lambda - 2 \kappa s)^2 \sin^2 2\beta}{4 s^2 (A_\lambda + \kappa s)^2 + v^2 (A_\lambda - 2 \kappa s)^2 \sin^2 2\beta}, \quad (15)$$

and arrive at the physical CP -odd states a_i (ordered in mass)

$$\begin{aligned} a_1 &= \cos \theta_A (\cos \beta H_{uI} + \sin \beta H_{dI}) + \sin \theta_A S_I, \\ a_2 &= -\sin \theta_A (\cos \beta H_{uI} + \sin \beta H_{dI}) + \cos \theta_A S_I. \end{aligned} \quad (16)$$

The lightest CP -odd particle a_1 is mainly composed of the singlet field when $\cos \theta_A \rightarrow 0$, and is a doublet field otherwise. Since we are looking for a very light scalar, we observe from the determinant of \mathcal{M}_{odd} that this occurs if A_κ and A_λ are small. This is technically natural since $A_\kappa, A_\lambda \rightarrow 0$ is a symmetry-enhancing limit.

The heavier CP -odd scalar mass is approximately

$$M_{a_2}^2 = \frac{2 \lambda s (A_\lambda + \kappa s)}{\sin 2\beta} + \frac{\lambda v^2 (A_\lambda - 2 \kappa s)^2 \sin 2\beta}{2 s (A_\lambda + \kappa s)}. \quad (17)$$

with the condition $A_\lambda + \kappa s > 0$.

For small A_λ and A_κ , we have the following approximate formulae:

$$M_{a_1}^2 \approx \frac{3 s (3 \lambda A_\lambda v^2 \sin 2\beta - 2 \kappa A_\kappa s^2)}{2(s^2 + v^2 \sin^2 2\beta)}, \quad (18)$$

$$M_{a_2}^2 \approx \frac{2 \kappa \lambda s^2}{\sin 2\beta} + 2 \kappa \lambda v^2 \sin 2\beta, \quad (19)$$

and

$$\tan \theta_A \approx \frac{s}{v \sin 2\beta}, \quad \cos^2 \theta_A \approx \frac{v^2 \sin^2 2\beta}{v^2 \sin^2 2\beta + s^2} \approx \frac{v^2 \sin^2 2\beta}{s^2}, \quad (20)$$

for $v \ll s$.

2.3 Interactions and decay modes

Since we are interested in dark matter annihilation through s -channel a_2 exchange, we list the relevant vertices associated with CP -odd scalars in this section. For $v \ll s$, the couplings of CP -odd scalars to fermions are

$$\begin{aligned} a_2 t_L t_R^c &: -i \frac{m_t \sin \theta_A}{\sqrt{2} v \tan \beta}, & a_2 b_L b_R^c &: i \frac{m_b \tan \beta \sin \theta_A}{\sqrt{2} v}, \\ a_1 t_L t_R^c &: -i \frac{m_t \cos \theta_A}{\sqrt{2} v \tan \beta}, & a_1 b_L b_R^c &: i \frac{m_b \tan \beta \cos \theta_A}{\sqrt{2} v}. \end{aligned} \quad (21)$$

The couplings of a_2 and a_1 to the lightest neutralino are

$$a_2 \chi \chi : \quad i g_{a_2 \chi \chi} \equiv i g_1 \sin \theta_A (\cos 2\beta \sin \alpha_1 - \sin 2\beta \sin \alpha_2), \quad (22)$$

$$a_1 \chi \chi : \quad i g_{a_1 \chi \chi} \equiv -i g_1 \cos \theta_A (\cos 2\beta \sin \alpha_1 - \sin 2\beta \sin \alpha_2), \quad (23)$$

with α_1 and α_2 defined in Eqs. (6–7). Therefore, the coupling of $a_2 \chi \chi$ increases as one increases the Higgsino components of the LSP. Their couplings to gauge bosons are

$$a_2(p) H^+(p') W_\mu^- : -\frac{i g_2 \sin \theta_A}{2} (p - p')_\mu, \quad (24)$$

$$a_1(p) H^+(p') W_\mu^- : \frac{i g_2 \cos \theta_A}{2} (p - p')_\mu, \quad (25)$$

$$a_2(p) h_1(p') Z_\mu : -\frac{i g}{\sqrt{2}} \sin \theta_A \cos(\alpha + \beta) (p' - p)_\mu \approx -\frac{i g}{\sqrt{2}} \frac{M_Z^2 \sin \theta_A \sin 4\beta}{2 M_{a_2}^2} (p' - p)_\mu, \quad (26)$$

$$a_1(p) h_1(p') Z_\mu : \frac{i g}{\sqrt{2}} \cos \theta_A \cos(\alpha + \beta) (p' - p)_\mu \approx \frac{i g}{\sqrt{2}} \frac{M_Z^2 \cos \theta_A \sin 4\beta}{2 M_{a_2}^2} (p' - p)_\mu. \quad (27)$$

The couplings among a_2 , a_1 and h_1 depend on the diagonalization of the CP -even scalar mass matrix, which may have significant one-loop contributions. For simplicity, we use the tree-level results in Eq. (11) to obtain analytic formulae. We arrive at the following dimensional couplings to the leading power in v/s [17]

$$a_1 a_1 h_1 : \quad w_{a_1 a_1 h_1} = \mathcal{O}(v^3/s^2), \quad (28)$$

$$a_2 a_1 h_1 : \quad w_{a_2 a_1 h_1} = -\sqrt{2} \kappa \mu + \mathcal{O}(\lambda^2 v^2/s). \quad (29)$$

Here the approximation is valid for small values of A_λ and A_κ . We also need the main decay channels of h_1 and a_2 . For the CP -even particle h_1 with a mass below $2 M_W$, it mainly decays into 2 a_1 's or 2 b 's with the decay widths calculated as following:

$$\Gamma(h_1 \rightarrow 2 a_1) = \frac{1}{32 \pi M_{h_1}} \mathcal{O}(v^6/s^4), \quad (30)$$

$$\Gamma(h_1 \rightarrow b + \bar{b}) \approx \frac{3 M_{h_1}}{8 \pi} \left(\frac{m_b}{\sqrt{2} v} \right)^2. \quad (31)$$

Thus for $v/s \ll 1$ the decay $h_1 \rightarrow 2 a_1$ is suppressed in favor of $h_1 \rightarrow b \bar{b}$. Note this suppression is directly connected to the small values of A_λ and A_κ . For large values of A_λ and A_κ , the $h_1 \rightarrow 2 a_1$ decay would be the dominant one [17].

Similarly for a_2 , if its mass is below twice the top quark mass, the leading two decay

channels are

$$\Gamma(a_2 \rightarrow h_1 a_1) \approx \frac{1}{32 \pi M_{a_2}} (\sqrt{2} \kappa \mu)^2 \approx \frac{\kappa \lambda}{32 \pi} M_{a_2} \sin 2\beta, \quad (32)$$

$$\Gamma(a_2 \rightarrow b + \bar{b}) \approx \frac{3 M_{a_2}}{8 \pi} \left(\frac{m_b \tan \beta \sin \theta_A}{\sqrt{2} v} \right)^2. \quad (33)$$

The bosonic decay channel can be dominant for modest values for κ and λ . However, if the a_2 mass exceeds twice the top quark mass, the decay channel into $t \bar{t}$ opens:

$$\Gamma(a_2 \rightarrow t + \bar{t}) \approx \frac{3 M_{a_2}}{8 \pi} \left(\frac{m_t \sin \theta_A}{\sqrt{2} v \tan \beta} \right)^2 \sqrt{1 - \frac{4 m_t^2}{M_{a_2}^2}}, \quad (34)$$

and this would become the dominant decay for a_2 assuming $\kappa, \lambda < 1$.

2.4 Spectrum from numerical calculations

In this section we find NMSSM model points that can provide the neutralino as a DM candidate to explain PAMELA. There are two relevant possibilities depending on the mass of a_1 :

1. The mass of the lightest CP -odd particle a_1 is in the range $(2 m_\mu, 1 \text{ GeV})$.
2. The mass of the lightest CP -odd particle a_1 is in the range $(2 m_\tau, 2 m_b)$.

In the first case a_1 mainly decays to two muons because decays to mesons are kinematically suppressed.¹ In the second case, because the couplings of a_1 to fermions are proportional to fermion masses, we anticipate that a_1 decays mainly to 2 τ 's. We do not consider the case that a_1 mainly decays into two electrons because of stringent constraints from the beam-dump experiment at CERN [18].

To find the interesting parts of the parameter space, we use the program NMHDECAY [15] for numerical checks. There are many experimental constraints considered in

¹Because a_1 is CP -odd, decays to two pions are forbidden due to CP symmetry, while decays to three pions are suppressed by the three-body phase space. In the following, we will approximate $a_1 \rightarrow 2\mu$ as 100% for case 1.

NMHDECAY such as various Higgs searches at LEP, $b \rightarrow s \gamma$ and $\Upsilon(1S) \rightarrow a_1 \gamma$. The model points presented in this paper pass all of the constraints embedded in NMHDECAY. Furthermore, we will discuss updated constraints on $\Upsilon(3S) \rightarrow a_1 \gamma \rightarrow \mu^+ \mu^- \gamma$ from BaBar and searches for dimuon resonances at LEP and Tevatron in section 7.

For both cases, in order to isolate the dark matter discussion, we choose the less relevant soft terms to be heavy. For example, we choose 500 GeV soft masses for sleptons, 1 TeV for squarks, 1 TeV for gluino and -2.5 TeV for all the A -terms in the quark and lepton sectors. We have used the updated top quark mass $m_t = 173.1 \pm 0.6 \pm 1.1$ GeV [19], which has a significant correlation to the Higgs boson mass for small $\tan \beta$ as considered in this paper.

For the muon-favored case, we choose values for other parameters in the NMSSM as in Table 1, which also shows the relevant spectrum and branching ratios of the light scalars.²

$\tan \beta$	λ	κ	A_λ	A_κ	μ_{eff}	M_1	M_2
3.1	0.24	0.194	-0.05	-0.273	-190	178.5	200
m_χ	M_{a_1}	M_{a_2}	M_{h_1}	M_{h_2}	M_{H^\pm}	m_{χ^\pm}	Γ_{a_2}
161.8	0.81	320.1	114.7	297.6	325.4	175.6	0.22
$\text{Br}(h_1 \rightarrow b\bar{b}) = 78.3\%$			$\text{Br}(h_1 \rightarrow \tau\bar{\tau}) = 8.1\%$		$\text{Br}(h_1 \rightarrow a_1 a_1) = 1.0\%$		
$\text{Br}(a_1 \rightarrow \mu^+ \mu^-) \approx 100\%$							
$\text{Br}(a_2 \rightarrow a_1 h_1) = 68.0\%$			$\text{Br}(a_2 \rightarrow b\bar{b}) = 22.5\%$		$\text{Br}(a_2 \rightarrow Z h_1) = 5.4\%$		
$\chi = -0.595(-i\lambda_1) + 0.347(-i\lambda_2) + 0.599(\psi_u^0) + 0.404(\psi_d^0) - 0.061(\psi_s) \quad \cos \theta_A = 0.12$							

Table 1: μ -favored model point. Masses are in GeV.

As can be seen from Table 1, if a_2 can be produced from $\chi\chi$ annihilation through the

²The default lower limit on the a_1 mass is 1 GeV in NMHDECAY. One has to change the code file named `mhiggs.f` to obtain an a_1 mass below 1 GeV.

resonance effect, the final products of the DM annihilation mainly contain $a_1 + h_1$. The a_1 decays into two muons to provide the positrons needed to explain the excess at PAMELA. The dark matter mass is mainly controlled by the parameter M_1 in this model, which is chosen to have the lightest neutralino mass below the top quark mass. Otherwise, a_2 will decay into $t\bar{t}$ with a significant branching ratio, and the neutralino annihilation produces a limited amount of positrons and lots of hadrons, the hadrons being disfavored by the null antiproton excess at PAMELA. It is intriguing that a combination of NMSSM and PAMELA results forces us to have a dark matter mass below around 170 GeV.

It is technically natural to have M_{a_1} below 1 GeV for tiny values of A_λ and A_κ as reported here, since the $U(1)_R$ symmetry protects its mass (one can also use the $U(1)_{PQ}$ symmetry to obtain a light pseudoscalar, see [20] for example). Notice that the branching ratio of $h_1 \rightarrow a_1 a_1$ is below 1.2% to satisfy the current null results of searches of a_1 in the channel $h_1 \rightarrow a_1 a_1 \rightarrow 4\mu$ at D0 (see Section 7.2).

For the tau-favored case, we list the values of model parameters, spectrum of particles and interesting branching ratios of light scalars in Table 2. The current direct searches only impose mild constraints on the model parameters. Therefore, we choose one representative point in the parameter space to have $h_1 \rightarrow a_1 a_1 \rightarrow 4\tau$ as the main decay channel of h_1 , and hence to have six τ 's in the final state of dark matter annihilations.

3 Dark matter annihilation cross section

Our first goal is to look for parameter space in the NMSSM having leptons as the main dark matter annihilation products. This goal can be achieved if the lightest CP -odd scalar is an intermediate annihilation product and subsequently decays to two taus or two muons from kinematic constraints. The other goal is to have a large dark matter annihilation cross section to explain the size of the PAMELA excess. The annihilation cross section can be enhanced through s -channel resonance effects. Assuming the lightest neutralino is the dark matter candidate in the NMSSM, the heavier CP -odd scalar a_2 is the only particle which can play this role. The CP -even scalars are ruled out by the CP symmetry, because the

$\tan \beta$	λ	κ	A_λ	A_κ	μ_{eff}	M_1	M_2
2.0	0.519	0.458	-14.83	-3.6	-200.0	162.25	1000
m_χ	M_{a_1}	M_{a_2}	M_{h_1}	M_{h_3}	M_{H^\pm}	m_{χ^\pm}	Γ_{a_2}
161.7	7.8	322.0	123.0	296.9	304.7	208.0	0.79
$\text{Br}(h_1 \rightarrow a_1 a_1) = 92.2\%$			$\text{Br}(h_1 \rightarrow b\bar{b}) = 7.6\%$				
$\text{Br}(a_1 \rightarrow \tau^+ \tau^-) = 85.0\%$			$\text{Br}(a_1 \rightarrow gg) = 7.7\%$			$\text{Br}(a_1 \rightarrow c\bar{c}) = 5.4\%$	
$\text{Br}(a_2 \rightarrow a_1 h_1) = 95.5\%$			$\text{Br}(a_2 \rightarrow b\bar{b}) = 2.8\%$			$\text{Br}(a_2 \rightarrow a_1 h_2) = 0.7\%$	
$\chi = 0.968 (-i\lambda_1) + 0.003 (-i\lambda_2) - 0.236 (\psi_u^0) - 0.080 (\psi_d^0) + 0.043 (\psi_s)$							

Table 2: τ -favored sample model point. The masses are in GeV.

initial state with two identical Majorana fermions is CP -odd. The lighter CP -odd scalar a_1 is far below the necessary mass region for the resonance effect.

Having established $\chi\chi \rightarrow a_2 \rightarrow X$ as the main dark matter annihilation channel, the main annihilation products are equivalent to the decay products of a_2 . The main dark matter annihilation products are shown in Fig. 1 for the two cases exemplified by Table 1 and Table 2.

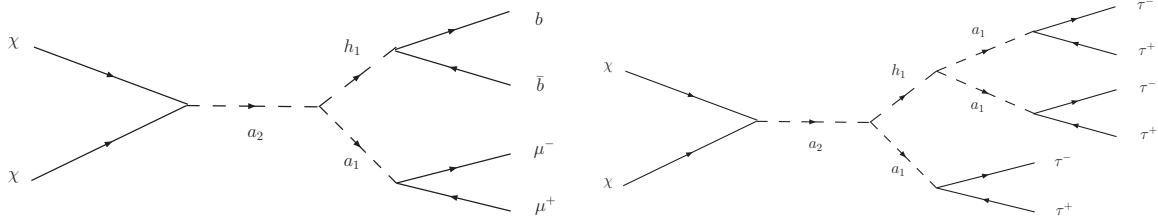


Figure 1: The Feynman diagram of the dominant neutralino annihilation channel. The left panel is for the muon-favored case, while the right panel is for the tau-favored case.

To calculate the dark matter annihilation cross section, we will concentrate on the main annihilation channel $\chi\chi \rightarrow a_2 \rightarrow a_1 h_1$, which is true for both two cases. The annihilation rate is

$$\sigma(\chi\chi \rightarrow a_2 \rightarrow a_1 h_1) v_{dm} = \frac{g_{a_2\chi\chi}^2 w_{a_1 a_2 h_1}^2}{16\pi [(M_{a_2}^2 - 4m_\chi^2)^2 + \Gamma_{a_2}^2 M_{a_2}^2]} \left(1 - \frac{M_{h_1}^2}{4m_\chi^2}\right), \quad (35)$$

up to $\mathcal{O}(v_{dm}^2/c^2)$ where the average dark matter speed is $v_{dm}/c \sim 10^{-3}$ in the galactic halo. Here the mass of a_1 is neglected and the coupling $w_{a_1 a_2 h_1}$ has mass dimension one. The co-annihilation effects can be neglected here, because other superpartner masses are much larger than the LSP mass. For the parameter points in Table 1 and Table 2, we have $\sigma(\chi\chi \rightarrow a_1 h_1) v_{dm}$ approximately 135 pb·c and 301 pb·c, respectively. Also from Table 1 and Table 2, the width Γ_{a_2} of a_2 is below 1 GeV, so the width part in the denominator of Eq. (35) can be neglected for $|M_{a_2} - 2m_\chi| > 1$ GeV considered here. Therefore, a large dark matter annihilation cross section can easily be obtained for the case of $m_\chi < m_t$. On the contrary, if $m_\chi > m_t$, the decay channel of $a_2 \rightarrow t\bar{t}$ is open and the decay width of a_2 is of order 10 GeV. Then the dark matter annihilation cross section is limited by the width part in Eq. (35), generically below 10 pb·c and not large enough to explain the PAMELA data. Thus we have *two* reasons to believe that the lightest neutralino mass is below the top quark mass: one is to have dominantly leptonic annihilation final states and the other one is to have a large annihilation cross section.

Our annihilation rates are by far larger than the necessary one (~ 1 pb·c) to satisfy the dark matter thermal relic density. One possible explanation for this discrepancy is that the dark matter is nonthermal. For example, other long-lived particles like the gravitino or moduli can decay into the LSP at a later time [10]. As argued in [10], a long-lived modulus field with a lifetime shorter than one second can naturally appear in the anomaly-mediated SUSY breaking model. The main dark matter relic abundance will be determined by the moduli annihilation cross section, which in principle can be smaller than the one for the neutralino and provide the observed dark matter relic density at the current time.

4 Positron excesses from neutralino annihilation

We now calculate the positron spectrum out of dark matter annihilation and compare it with the PAMELA results to determine the PAMELA-favored parameter space in the NMSSM. We first discuss the source term of primary positrons from DM annihilations, propagation of cosmic ray positrons and then the positron fluxes measured at PAMELA. We also consider the charge-dependent solar modulation on the positron fraction spectrum.

4.1 The source term for primary positrons

For the two cases we are considering in this paper, the source term for primary positrons can be generally written as:

$$q(\mathbf{x}, E) = \frac{1}{2} \langle \sigma v \rangle \left(\frac{\rho(\mathbf{x})}{m_\chi} \right)^2 \frac{dN_{e^+}}{dE_{e^+}}. \quad (36)$$

Here the overall factor $1/2$ is from the Majorana property of the neutralino DM candidate; $\langle \sigma v \rangle$ is the thermally averaged annihilation cross section and to a good approximation can be replaced by the formula in Eq. (35); dN_{e^+}/dE_{e^+} is the energy spectrum of positrons; $\rho(\mathbf{x})$ is the dark matter distribution inside the Milky Way halo. For the dark matter distribution we use either the Navarro, Frenk and White (NFW) profile [21] or the cored isothermal (ISO) profile [22]; the use of other profiles may change discussions in this paper, especially for the gamma ray spectrum. The NFW and ISO profiles are parametrized as:

$$\rho_{\text{NFW}}(r) = \rho_\odot \left(\frac{r_\odot}{r} \right) \left(\frac{r_s + r_\odot}{r_s + r} \right)^2, \quad \rho_{\text{ISO}}(r) = \rho_\odot \left(\frac{r_s^2 + r_\odot^2}{r_s^2 + r^2} \right), \quad (37)$$

with $r_s = 20$ kpc (NFW), 5 kpc (ISO) is the radius of the central core; $r_\odot = 8.5$ kpc is the galactocentric distance of the solar system; $\rho_\odot = 0.3 \text{ GeV cm}^{-3}$ is the solar neighborhood DM density.

The positron energy spectrum function for the μ case can be generally expressed as

$$\begin{aligned} \frac{dN_{e^+}}{dE_{e^+}} &= \int dE_{a_1} dE_{\mu^+} \frac{dN_{a_1}}{dE_{a_1}} \mathcal{P}(E_{a_1} \rightarrow E_{\mu^+}) \mathcal{P}(E_{\mu^+} \rightarrow E_{e^+}) \\ &+ 2 \int dE_{h_1} dE_{a_1} dE_{\mu^+} \frac{dN_{h_1}}{dE_{h_1}} \mathcal{P}(E_{h_1} \rightarrow E_{a_1}) \mathcal{P}(E_{a_1} \rightarrow E_{\mu^+}) \mathcal{P}(E_{\mu^+} \rightarrow E_{e^+}). \end{aligned} \quad (38)$$

Here $\mathcal{P}(E_i \rightarrow E_j)$ denotes the probability of a particle i with energy E_i decaying into a particle j with energy E_j ; the factor of 2 in the expression is because h_1 decays into 2 a_1 's. We neglect the positrons and electrons from the b quark decays although the h_1 mainly decays into two b quarks in the muon-favored case. Because positrons and electrons from b decays are relatively soft, including them makes only a slight change in the spectrum below 10 GeV, where the background is anyway dominant.

From two χ 's annihilating into a_1 and h_1 , and neglecting the mass of a_1 , we have

$$\begin{aligned}\frac{dN_{a_1}}{dE_{a_1}} &= \text{Br}(a_2 \rightarrow h_1 a_1) \delta\left(E_{a_1} - (m_\chi - \frac{M_{h_1}^2}{4m_\chi})\right), \\ \frac{dN_{h_1}}{dE_{h_1}} &= \text{Br}(a_2 \rightarrow h_1 a_1) \delta\left(E_{h_1} - (m_\chi + \frac{M_{h_1}^2}{4m_\chi})\right).\end{aligned}\quad (39)$$

Since the emission of muons in the a_1 rest frame and the emission of a_1 's in the h_1 rest frame are isotropic, we have

$$\mathcal{P}(E_{a_1} \rightarrow E_{\mu^+}) \approx \frac{1}{E_{a_1}} \mathcal{H}(E_{a_1} - E_{\mu^+}), \quad \mathcal{P}(E_{h_1} \rightarrow E_{a_1}) \approx \frac{\text{Br}(h_1 \rightarrow a_1 a_1)}{E_{h_1}}, \quad (40)$$

with $\mathcal{H}(x)$ is the heavy-side function and the masses of μ^+ and a_1 are neglected in the approximation formula. Neglecting the muon polarization, the positron energy probability in muon decay has the following analytic form [4]

$$\mathcal{P}(E_{\mu^+} \rightarrow E_{e^+}) = \frac{1}{3 E_{\mu^+}} \left[5 - 9 \left(\frac{E_{e^+}}{E_{\mu^+}} \right)^2 + 4 \left(\frac{E_{e^+}}{E_{\mu^+}} \right)^3 \right] \mathcal{H}(E_{\mu^+} - E_{e^+}). \quad (41)$$

Here the functions $\mathcal{P}(E_i \rightarrow E_j)$ are normalized such that $\int dE_j \mathcal{P}(E_i \rightarrow E_j) = \text{Br}(i \rightarrow j)$.

The τ -favored case is more complicated than the μ -case, because other than leptonic channels τ can also decay to various charged mesons, which decay eventually to electrons and positrons. In order to obtain the electron energy dependent probability from τ decays, we use **PYTHIA** [23], which calls the program **TAUOLA** [24], to simulate the inclusive electron/positron energy spectrum from both direct and indirect τ decays. As can be seen from Fig. 2, once the energy of the (unpolarized) τ is much larger than its mass, the fractional

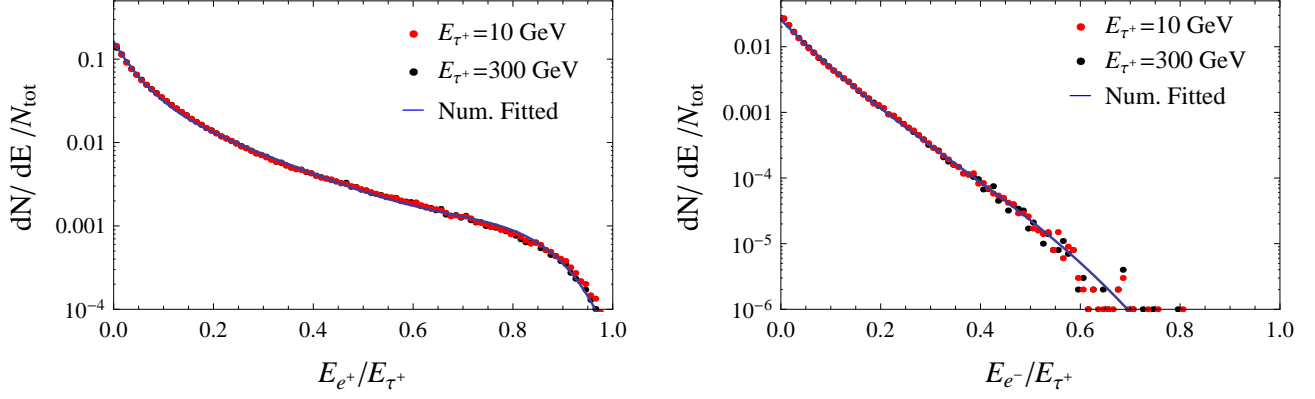


Figure 2: Left panel: the positron energy spectrum from inclusive tau decays. The red and the black points are for 10 GeV and 300 GeV τ^+ energy, respectively. The blue line is from a fitted analytic function in the text. Right panel: similar as the left panel, but for electrons. On average, 1.16 positrons and 0.16 electrons are generated from one τ^+ decay.

electron and positron energy spectra are independent of the energy of the τ . The large fluctuations for $E_{e^-}/E_{\tau^+} > 0.5$ in the right panel of Fig. 2 are due to limited Monte Carlo statistics. The tiny fraction of e^- out of τ^+ for $E_{e^-}/E_{\tau^+} > 0.5$ can be understood from the fact that only high multiplicity final states can contain an e^- with a different charge from τ^+ .

For these e^+ and e^- spectra from inclusive τ^+ decays, the following fitted functions provide good agreement:

$$\begin{aligned}\mathcal{P}(E_{\tau^+} \rightarrow E_{e^+}) &= \frac{1}{E_{\tau^+}} e^{-97.716 x^5 + 223.389 x^4 - 193.748 x^3 + 82.595 x^2 - 22.942 x + 2.783} \mathcal{H}(1 - x), \\ \mathcal{P}(E_{\tau^+} \rightarrow E_{e^-}) &= \frac{1}{E_{\tau^+}} e^{-15.575 x^3 + 15.79 x^2 - 18.083 x + 0.951} \mathcal{H}(1 - x),\end{aligned}\tag{42}$$

with $x = E_{e^\pm}/E_{\tau^+}$. For each τ^+ , on average, there are $\int dE_{e^+} \mathcal{P}(E_{\tau^+} \rightarrow E_{e^+}) \approx 1.16$ positrons and $\int dE_{e^-} \mathcal{P}(E_{\tau^+} \rightarrow E_{e^-}) \approx 0.16$ electrons produced in the decay. When a_1 decays into $\tau^+ + \tau^-$, there are on average 1.32 positrons out of a single a_1 decay. Therefore, we insert Eq. (42) into the analogous formula in Eq. (38) for the τ case.

4.2 Propagation of positrons and electrons

The propagation of positrons and electrons in the galactic medium is described by the following transport equation:

$$\frac{\partial N}{\partial t} - \nabla \cdot [K(\mathbf{x}, E) \nabla N] - \frac{\partial}{\partial E} [b(E) N] = q(\mathbf{x}, E), \quad (43)$$

where $N(\mathbf{x}, E)$ denotes the positron number density per unit energy; $q(\mathbf{x}, E)$ is the positron source term; $K(\mathbf{x}, E) = K_0 (E/E_0)^\delta$ is the diffusion constant with $E_0 \equiv 1$ GeV; $b(E) = E^2/(E_0 \tau_E)$ is the positron energy synchrotron and inverse Compton loss rate with $\tau_E = 10^{16}$ s. The diffusive halo is modeled as a cylinder with radius $r_s = 20$ kpc and the vertical direction z inside $(-L, L)$. The half thickness is not constrained and varies from 1 to 15 kpc. We will consider three different parameter points for the cosmic ray propagation model in Table 3. Those sets of propagation parameters are compatible with the secondary/primary

Model	δ	K_0 [kpc ² /Myr]	L [kpc]
MIN (M2)	0.55	0.00595	1
MED	0.70	0.0112	4
MAX (M1)	0.46	0.0765	15

Table 3: Three combinations of cosmic ray propagation parameters, which give the minimum, median and maximum positron fluxes [25].

test for the secondary and primary antiprotons [26]. Assuming a time-independent state and considering the diffusion constant as space independent, we have

$$- K_0 \left(\frac{E}{E_0} \right)^\delta \Delta N - \frac{\partial}{\partial E} \left[\frac{E^2}{E_0 \tau_E} N \right] = q(\mathbf{x}, E). \quad (44)$$

Defining a pseudo-time and a relative pseudo-time between the source point and the observation point, respectively, as

$$\hat{t}(E) \equiv \tau_E \frac{(E/E_0)^{\delta-1}}{1-\delta}, \quad \hat{\tau}(E, E_S) = \hat{t}(E) - \hat{t}(E_S), \quad (45)$$

the characteristic diffusion length in the radial direction is

$$\lambda_D(E, E_S) \equiv \sqrt{4 K_0 \hat{\tau}(E, E_S)}. \quad (46)$$

In Ref. [25], an analytic solution for the positron flux on the Earth has been obtained and has the following form:

$$\phi_{e^+}^\odot(E) = \frac{\beta c}{4\pi} \int_E^\infty dE_s q(r_\odot, E_s) \times \frac{\tau_E E_0}{E^2} \times \eta(\lambda_D(E, E_S)). \quad (47)$$

Using the Bessel expansion method, the halo integral η , which is the volume integration of the Green function of Eq. (44), has both radial and vertical expansions:

$$\eta(\lambda_D) = \sum_{i=1}^\infty \sum_{n=1}^\infty J_0(x_i r_\odot / r_s) \sin\left(\frac{n\pi}{2}\right) \exp\left[-\left(\left(\frac{n\pi}{2L}\right)^2 + \left(\frac{x_i}{r_s}\right)^2\right) \frac{\lambda_D^2}{4}\right] R_{i,n}, \quad (48)$$

with

$$R_{i,n} = \frac{2}{J_1(x_i)^2 r_s^2} \int_0^{r_s} dr r J_0(x_n r / r_s) \frac{1}{L} \int_{-L}^{+L} dz \sin\left(\frac{n\pi z}{2L}\right) \left(\frac{\rho(\sqrt{r^2 + z^2})}{\rho_\odot}\right)^2. \quad (49)$$

Here J_k is the Bessel function of the first kind and x_i is the i -th root of the J_0 Bessel function. In practice, one can use the numerically fitted functions in Ref. [27] to speed up the numerical calculations. For example, we use the following numerical function for the NFW dark matter profile and the MIN (M2) propagation model:

$$\eta(\lambda_D) = 0.5 + 0.774 \tanh\left(\frac{0.096 - \ell}{0.211}\right) \left[-0.448 \exp\left(-\frac{(\ell - 192.8)^2}{33.88}\right) + 0.649\right], \quad (50)$$

with $\ell \equiv \log_{10}(\lambda_D/\text{kpc})$.

4.3 Solar modulation

PAMELA has measured the positron over electron fraction with energy below 10 GeV, and obtained a spectrum significantly below the background fitted from other cosmic ray experiments. One possible explanation of this discrepancy is due to the charge sign dependence of the solar modulation. The magnetic field of the solar wind is dominated by the dipole term, and the projection of this dipole on the solar rotation axis can be either positive or negative, called A^+ and A^- states, respectively. At each sunspot maximum, the dipole reverses its direction and leads to a periodic function for the dipole magnetic field with a roughly 12 year period.³

Using two functions $c_+(E)$ and $c_-(E)$ to model the solar modulation, we have the observed positron fraction on the Earth as:

$$F_{\oplus}^{\pm}(E) = \frac{c_{\pm}(E) \Phi_{e^+}(E)}{c_{\pm}(E) \Phi_{e^+}(E) + c_{\mp}(E) \Phi_{e^-}(E)}, \quad (51)$$

with $+$ for the solar system in the A^+ state and $-$ for the A^- state. Here $\Phi_{e^{\pm}}(E)$ denote the positron/electron fluxes. One notices that only the ratio of $c_+(E)/c_-(E)$ is relevant for the positron fraction. The ratio of the total electron flux in the A^+ cycle to total electron flux at a similar phase in the A^- cycle is

$$R(E) = \frac{c_+(E) \Phi_{e^+}(E) + c_-(E) \Phi_{e^-}(E)}{c_-(E) \Phi_{e^+}(E) + c_+(E) \Phi_{e^-}(E)}. \quad (52)$$

This ratio can be fitted in principle from the data shown in Fig. 5 of Ref. [28]. However, since the lower energy bins of PAMELA (where the contribution from dark matter is negligible) are measured so precisely, one can use the data from PAMELA (A^- cycle) and the known background [29] (without an assumption of solar modulation) to determine this ratio. The following fitted formula can achieve the goal:

$$R(E) = \max [\min (0.48 + 0.27 \log(E/\text{GeV}), 1.0), 0.2], \quad (53)$$

which will be used in our following analysis about the comparison of model predictions and PAMELA data. The general form of this expression is suggested by Ref. [30]. Eventually one

³Figure 1 of Ref. [28] shows clear evidence for this behavior in the electron flux.

needs to understand or to calculate this ratio function or $c_{\pm}(E)$ from first principles. Due to the magnitude of the solar magnetic field, only positrons/electrons with energy below about 10 GeV can be influenced by the solar wind. $R(E)$ is a monotonically increasing function and saturates at unity above 7 GeV.

In terms of $R(E)$ and $F(E) \equiv \Phi_{e^+}(E)/(\Phi_{e^-}(E) + \Phi_{e^+}(E))$, which is the positron fraction without solar modulation effects, one has:

$$F_{\oplus}^-(E) = \frac{F^2(R+1) - FR}{2F-1}, \quad F_{\oplus}^+(E) = \frac{F^2(R+1) - F}{R(2F-1)}. \quad (54)$$

4.4 PAMELA positron excess

Before we compare the positrons from the neutralino annihilations in the NMSSM to the PAMELA results, we first discuss the electron and positron backgrounds from standard astrophysical processes. Background positrons are mostly secondaries originating from spallation processes of cosmic rays, mostly primary protons, off the interstellar gas, thus mainly occurring in the galactic disk. The primary electrons are mainly produced by shock wave acceleration in supernovae. To simplify our comparison of model predictions to experimental data (without the solar modulation effects), we use the following numerically fitted formulae for the background [30], which agrees with the full results calculated in [29]:

$$\begin{aligned} \phi_{\text{prim,bkg}}^{e^-} &= \frac{0.16 E^{-1.1}}{1 + 11 E^{0.9} + 3.2 E^{2.15}} \text{GeV}^{-1} \text{cm}^{-2} \text{s}^{-1} \text{sr}^{-1}, \\ \phi_{\text{sec,bkg}}^{e^-} &= \frac{0.70 E^{0.7}}{1 + 110 E^{1.5} + 600 E^{2.9} + 580 E^{4.2}} \text{GeV}^{-1} \text{cm}^{-2} \text{s}^{-1} \text{sr}^{-1}, \\ \phi_{\text{sec,bkg}}^{e^+} &= \frac{4.5 E^{0.7}}{1 + 650 E^{2.3} + 1500 E^{4.2}} \text{GeV}^{-1} \text{cm}^{-2} \text{s}^{-1} \text{sr}^{-1}, \end{aligned} \quad (55)$$

with E in GeV. Combining the background and signal positrons, we have a general formula for the positron fraction

$$F_{\oplus}^- = \frac{c_- \phi(e^+)}{c_+ \phi(e^-) + c_- \phi(e^+)} = \frac{c_- (\phi_{\text{sec,bkg}}^{e^+} + \phi_{\text{sig}}^{e^+})}{c_+ (\phi_{\text{prim,bkg}}^{e^-} + \phi_{\text{sec,bkg}}^{e^-} + \phi_{\text{sig}}^{e^-}) + c_- (\phi_{\text{sec,bkg}}^{e^+} + \phi_{\text{sig}}^{e^+})}, \quad (56)$$

assuming that the PAMELA data were taken when the sun is in the A^- cycle.

Using the model point and the masses of χ , h_1 and a_1 reported in Table 1, we have the positron excess for the μ -favored model point in the NMSSM shown in Fig. 3. To generate the

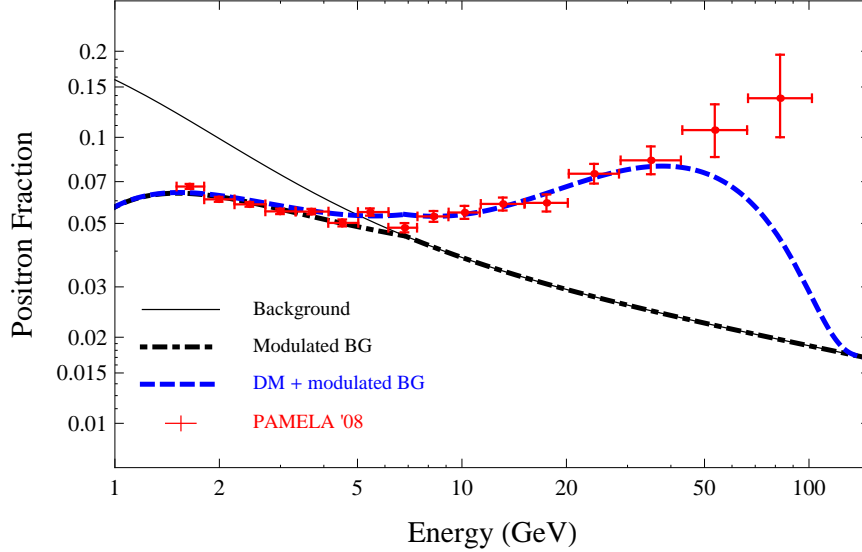


Figure 3: The positron fraction from the μ -favored model point in the NMSSM. The solid black line is the background without considering solar modulation. The dot-dashed black line is the background with the solar modulation effects. The dashed blue line is the positron fraction from neutralino ($m_\chi = 162$ GeV) annihilations plus the modulated background. The red points are data from PAMELA with one standard deviation errors. The dark matter annihilation cross section is $6.0 \times 10^{-24} \text{ cm}^3 \text{ s}^{-1}$. The MIN propagation model is used here.

plot in Fig. 3, we have used the MIN propagation model from Table 3, which provides a best fit to the PAMELA data. The other two propagation models generate a flatter curve than the MIN model. This is because as the thickness of the diffusive halo decreases, the positrons detected on the Earth originate from a nearby region (the characteristic propagation distance λ_D decreases), and hence low-energy positrons are less likely to reach the Earth. This leads to a steeper spectrum for the MIN propagation model. Since all three propagation models are supported by the N-body simulation, the combination of the NMSSM and the PAMELA data (assuming the NMSSM interpretation was confirmed by, e.g. collider discoveries) could

help to determine a correct galaxy model.

In Fig. 3 we note that the NMSSM model is 3 sigma below the PAMELA data point in the highest energy bin. However the overall agreement is quite good. To estimate the goodness of fit conservatively, we ignore the PAMELA data below 7.4 GeV, which should have negligible contribution from the dark matter annihilation, and calculate the averaged χ^2 for the 8 bins above 7.4 GeV:

$$\frac{\chi^2}{8} = \frac{1}{8} \sum_{i=1}^8 \left(\frac{x_i^{\text{model}} - x_i^{\text{exe}}}{\sigma_i} \right)^2 \approx 0.9. \quad (57)$$

If the neutralino annihilation in the NMSSM is the explanation for the PAMELA data, the rising feature of the positron fraction spectrum should end at around 70 GeV. This is a dramatic prediction for future PAMELA results. This predicted turnover follows uniquely from the requirement in the NMSSM model that the dark matter LSP mass cannot exceed the top quark mass.

For completeness, we also show the electron plus positron energy spectrum from dark matter annihilation in Fig. 4. We also include the latest results from Fermi LAT in the red and crossed points [31] in Fig. 4. There is an additional uncertainty from the LAT energy scale, which can shift the whole gray band by 5% (up) to 10% (down) and is not shown in this figure. In this figure the electron and positron fluxes from the background in Eq. (55) plus signal have been normalized to agree with the first bin of Fermi LAT. The positron fraction predictions from PAMELA are unchanged by this manipulation.

The agreement between the predicted electron+positron spectrum and the Fermi LAT data is about the same with and without adding the NMSSM signal. The generally poor agreement should thus be attributed to a defect in our understanding of the cosmic electron/positron background. More generally, we conclude that a neutralino annihilation explanation for PAMELA is consistent with the Fermi LAT results, as long as the extra contribution to the electron+positron spectrum is within the Fermi LAT errors.

Having discussed the μ -favored point in the NMSSM, we also report the results for the τ -favored point. It turns out that although τ -favored points can be found easily in the parameter space of the NMSSM, they provide a worse fit to the PAMELA data. This is

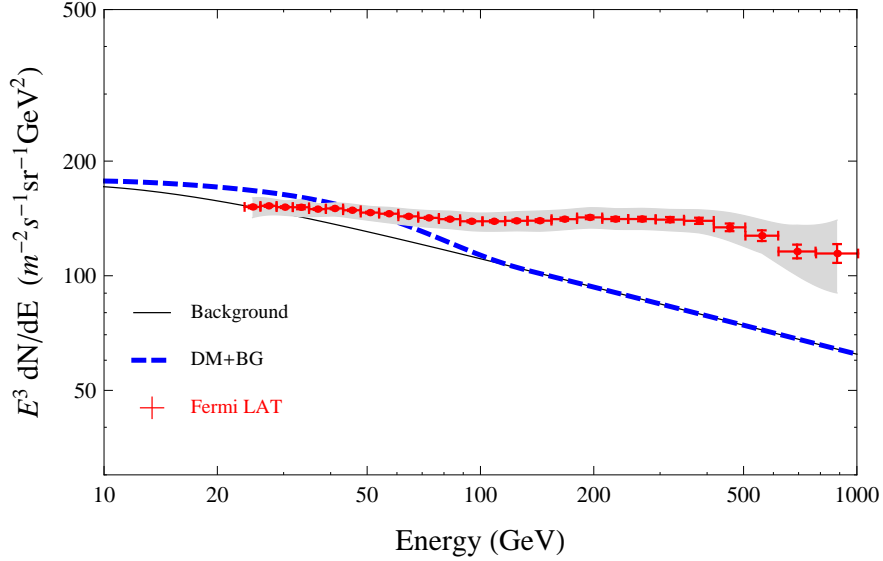


Figure 4: The electron plus positron spectrum from the μ -favored model. The solid black line is the background. The dashed blue line is from the neutralino annihilation plus the background. The red crossed points are the results from Fermi Large Area Telescope (Fermi LAT) with the gray band for systematic errors. The dark matter annihilation cross section is $6.0 \times 10^{-24} \text{ cm}^2 \text{ s}^{-1}$. The MIN propagation model is used here.

mainly because the positrons from τ^+ decays are softer than the positrons from μ^+ decays. This fact can be seen from the right panel of Fig. 5, where a comparison between μ and τ cases is shown. Only taking the PAMELA data above 7.4 GeV into account, we calculate the average χ^2 for the fit of this τ -favored model point to PAMELA data as $\chi^2/8 \approx 3.4$. Because of this large χ^2 , we will concentrate on the μ -favored model from here on.

5 PAMELA antiproton

Since there is no excess of the antiproton fraction observed at PAMELA, this imposes constraints on the antiproton production cross section from dark matter annihilation. Specifically to the muon-favored case in the NMSSM, the dominant source of hadronic production

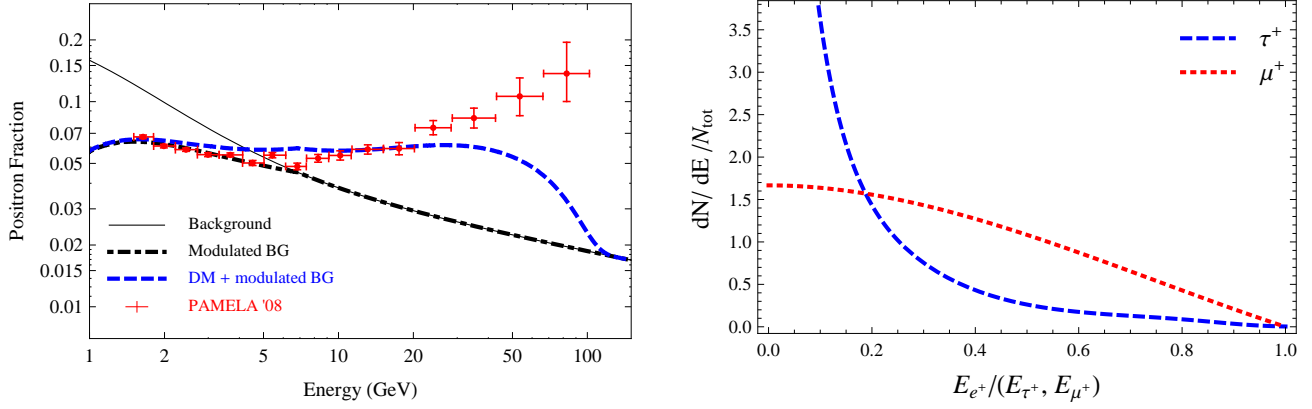


Figure 5: Left panel: the positron fraction from one τ -favored model point in the NMSSM. The dark matter ($m_\chi = 160$ GeV) annihilation cross section is $9.0 \times 10^{-24} \text{ cm}^2 \text{ s}^{-1}$. The MIN propagation model is used here. Right panel: a comparison of positron energy spectra from τ^+ decays and from μ^+ decays.

is from $h_1 \rightarrow b\bar{b}$ and $a_2 \rightarrow b\bar{b}$. Similarly to the calculations for the positron fraction spectrum, we first use an analytic function to fit the fragmentation function of $b\bar{b}$ to antiprotons. The antiproton energy spectra for two different $b\bar{b}$ center of mass energies are extracted using PYTHIA and shown in Fig. 6. We use the following fitted function later to replace the numerically simulated antiproton energy spectrum from h_1 decays:

$$\mathcal{P}(E_{h_1} \rightarrow b\bar{b} \rightarrow T_{\bar{p}}) = \frac{2}{E_{h_1}} e^{-307.05 x^5 + 525.86 x^4 - 331.51 x^3 + 96.71 x^2 - 28.56 x + 2.755}, \quad (58)$$

where $x = 2(T_{\bar{p}} + m_p)/E_{h_1}$. As is customary in antiproton cosmic ray analyses, we substitute the proton energy by its kinetic energy $T_{\bar{p}} = E_{\bar{p}} - m_p$ in the following. The antiproton spectrum from a_2 has a same formula replacing E_{h_1} with E_{a_2} .

The source term for antiprotons from DM annihilations is similar to Eq. (36) but substituting dN_{e^+}/dE_{e^+} with

$$\begin{aligned} \frac{dN_{\bar{p}}}{dT_{\bar{p}}} &= \int dE_{h_1} \frac{dN_{h_1}}{dE_{h_1}} \text{Br}(h_1 \rightarrow b\bar{b}) \mathcal{P}(E_{h_1} \rightarrow b\bar{b} \rightarrow T_{\bar{p}}) \\ &+ \int dE_{a_2} \frac{dN_{a_2}}{dE_{a_2}} \text{Br}(a_2 \rightarrow b\bar{b}) \mathcal{P}(E_{a_2} \rightarrow b\bar{b} \rightarrow T_{\bar{p}}). \end{aligned} \quad (59)$$

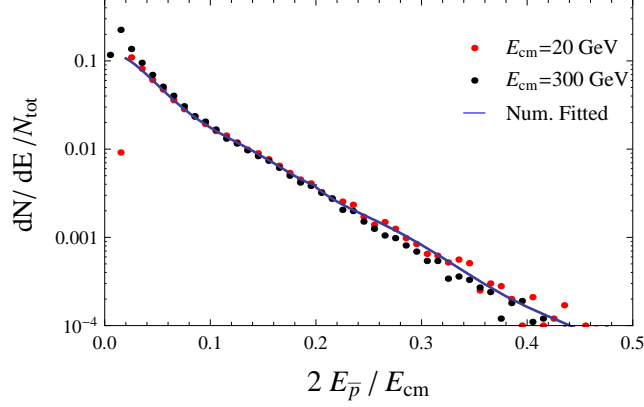


Figure 6: The $b\bar{b}$ to antiproton fragmentation function. The red and black points are for 20 GeV and 300 GeV $b\bar{b}$ center of mass energies. The blue line is from a fitted analytic function described in the text. The fragmentation function is extracted using PYTHIA.

However, due to the fact that $m_p \gg m_e$, the energy loss term for antiprotons can be neglected. The steady diffusion equation for antiprotons is [26]:

$$-K_p(T) \Delta N + \frac{\partial}{\partial z}(\text{sign}(z) V_c N) + 2h\delta(z)\Gamma_{\text{ann}} N = q(\mathbf{x}, T). \quad (60)$$

Here N is the number density of antiprotons per unit energy and $K_p(T) = K_0 \beta (p/\text{GeV})^\delta$ with β and p are the antiproton velocity and momentum. The second term is related to the convective wind, which has a direction outward from the galactic plane and represents the movement of the medium responsible for the antiproton diffusion. The velocity V_c is assumed to be constant and has values shown in Table 4 for different propagation models. The third term represents annihilations of antiprotons and interstellar protons in the galactic plane with a thickness $h = 0.1$ kpc. The annihilation rate between antiproton and protons is $\Gamma_{\text{ann}} = (n_{\text{H}} + 4^{2/3} n_{\text{He}}) \sigma_{p\bar{p}}^{\text{ann}} v_{\bar{p}}$ with $n_{\text{H}} \approx 1 \text{ cm}^{-3}$ and $n_{\text{He}} \approx 0.07 \text{ cm}^{-3}$. The $\sigma_{p\bar{p}}^{\text{ann}}$ as a function of antiproton kinetic energy is given in [32] and [33]: $661(1 + 0.0115 T^{-0.774} - 0.984 T^{0.0151})$ mb for $T < 15.5$ GeV and $36 T^{-0.5}$ mb for $T \geq 15.5$ GeV. This annihilation process is dominant at low energy and leads to a decreased flux of antiprotons with low energy. In our analysis, other non-annihilation interactions between antiprotons and the interstellar medium are

Model	δ	K_0 [kpc ² /Myr]	L [kpc]	V_c [km/s]
MIN	0.85	0.0016	1	13.5
MED	0.70	0.0112	4	12
MAX	0.46	0.0765	15	5

Table 4: Three combinations of cosmic ray propagation parameters, which give the minimum, median and maximum signal antiproton fluxes.

neglected. These effects are not important for the antiproton flux with energy above a few GeV.

Similar to the positron case, the diffusion equation for the antiproton can be solved analytically and has the following concise form as its solution [26]:

$$\phi_{\bar{p}}^{\odot}(T_{\bar{p}}) = \frac{\beta_{\bar{p}} c}{4\pi} \left(\frac{\rho_{\odot}}{m_{\chi}} \right)^2 \frac{1}{2} \langle \sigma v \rangle \frac{dN_{\bar{p}}}{dT_{\bar{p}}} \times R(T_{\bar{p}}). \quad (61)$$

Again the numerically fitted analytical formulae for $R(T_{\bar{p}})$ can be found in Ref. [27] for different halo and propagation models and will be used in our following calculations. For the MIN propagation model and the NFW dark matter profile, we have

$$R(T)/\text{Myr} = 10^{0.913 + 0.601 \log_{10}(T/\text{GeV}) - 0.309 \log_{10}(T/\text{GeV})^2 - 0.036 \log_{10}(T/\text{GeV})^3 + 0.0122 \log_{10}(T/\text{GeV})^4}. \quad (62)$$

To obtain the antiproton flux observed on the Earth, we need to take the solar modulation effect into account. The solar modulation effect is represented by a parameter ϕ , which is 500 MV for minimum solar activity when PAMELA was taking data. The energy spectrum of antiprotons on the Earth is

$$\phi_{\bar{p}}^{\oplus}(T_{\bar{p}}) = \phi_{\bar{p}}^{\odot}(T_{\bar{p}} + |Z|\phi) \frac{(T_{\bar{p}} + m_p)^2 - m_p^2}{(T_{\bar{p}} + |Z|\phi + m_p)^2 - m_p^2}, \quad (63)$$

with $Z = 1$ the electric charge of the antiproton.

The background for primary protons can be extrapolated from other cosmic ray experiments. Using the data from AMS [34], we arrive at the following fitted analytic function to describe the primary proton background:

$$\phi_p^{\text{BG,AMS}}(T) = e^{-0.00097 \log^5 T + 0.012 \log^4 T + 0.014 \log^3 T - 0.382 \log^2 T - 0.828 \log T + 6.88}, \quad (64)$$

with T in GeV and the flux in $\text{m}^{-2} \text{s}^{-1} \text{sr}^{-1} \text{GeV}^{-1}$. Similarly, from CAPRICE98 [35] data, we have

$$\phi_p^{\text{BG,CAPRICE}}(T) = e^{-0.0005 \log^5 T + 0.005 \log^4 T + 0.019 \log^3 T - 0.433 \log^2 T - 0.882 \log T + 6.89}, \quad (65)$$

The primary proton fluxes measured at AMS and CAPRICE can deviate from each other by a difference as large as 20%. We include both results in our analysis to encode uncertainties of our primary proton flux background. The secondary antiproton background can be found in the detailed analysis in [36] and fitted in [27] as:

$$\phi_{\bar{p}}^{\text{BG}}(T) = 10^{0.028 \log_{10}^4 T - 0.02 \log_{10}^3 T - 1.0 \log_{10}^2 T + 0.07 \log_{10} T - 1.64}. \quad (66)$$

A comparison of the antiproton/proton flux ratio from the neutralino annihilation and the PAMELA data is shown in Fig. 7. Noticing that the MIN propagation model provides a better fit to the PAMELA positron data, the model point in Table 1 is marginally allowed by the PAMELA antiproton data. To quantify the discrepancy between the model prediction and the PAMELA observed data, we calculate the χ^2 by including all bins. We also calculate the χ^2 between the background and PAMELA data. Using the background extrapolated from AMS, we have χ^2 to be 1.7 for the DM prediction plus the background and 3.6 for the background only. While, using the background from CAPRICE, we have χ^2 to be 3.8 for the DM prediction plus the background and 2.2 for the background only. We conclude that the model point in Table 1 is allowed by the PAMELA antiproton data, taking into account the large uncertainties of the background primary proton flux.

Although the branching ratio $\text{Br}(a_2 \rightarrow b\bar{b})$ is smaller than $\text{Br}(a_2 \rightarrow h_1 a_1)\text{Br}(h_1 \rightarrow b\bar{b})$, the center of mass energy of $b\bar{b}$ directly out of a_2 is approximately twice of the center of mass energy out of h_1 . Therefore, the large antiproton fraction for the kinetic energy above 10 GeV

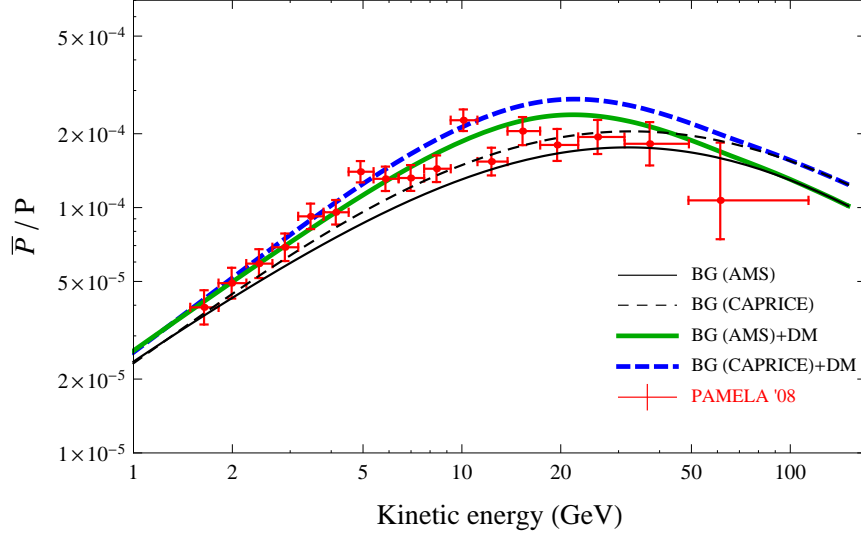


Figure 7: The antiproton-to-proton flux ratio as a function of kinetic energy. The black solid and dashed lines are the backgrounds from AMS and CAPRICE, respectively. The thick green solid line is from the dark matter annihilation plus the background (AMS) using the MIN propagation model. The thick blue dashed line is using the background (CAPRICE). The red crossed points are data from PAMELA. The neutralino mass is $m_\chi = 162$ GeV and its annihilation cross section is $6.0 \times 10^{-24} \text{ cm}^2 \text{ s}^{-1}$.

mainly comes from dark matter annihilating directly into $b\bar{b}$. To suppress the antiproton flux more efficiently, one could change the model parameters to suppress the branching ratio of a_2 to $b\bar{b}$. One simple way to do this is to reduce $\tan\beta$. However, by doing so, the branching ratio of $h_1 \rightarrow a_1 a_1$ is also increased, creating a tension with the upper limit from D0 described in Section 7.2.

6 Gamma ray fluxes for Fermi LAT

If the μ -favored model points in the NMSSM are the correct explanation of the PAMELA positron excess, there will be lots of associated gamma rays generated. Existing gamma ray data from HESS [37] and EGRET [38] can in principle impose constraints on the dark

matter annihilation cross section to electrons and positrons. Also, the recent and upcoming gamma-ray flux data from Fermi LAT have a smaller statistic uncertainty and can be used to test the PAMELA-favored NMSSM model.

The differential gamma-ray flux from the dark matter annihilation has the following general formula:

$$\frac{d^2\Phi_\gamma}{d\Omega dE_\gamma} = \frac{1}{2} \frac{\langle\sigma v\rangle}{4\pi m_\chi^2} \frac{dN_\gamma}{dE_\gamma} \int_0^\infty \rho^2(r) dl(\psi). \quad (67)$$

Here $r^2 = l^2 + r_\odot^2 - 2lr_\odot \cos\psi$ with ψ as the angle between the line of sight and the galactic plane. One can separate the astrophysical uncertainties by introducing the quantity

$$J(\psi) = \frac{1}{r_\odot \rho_\odot^2} \int_0^\infty \rho^2(r) dl(\psi). \quad (68)$$

Performing the solid angle integration, the differential gamma-ray flux is

$$\frac{d\Phi_\gamma}{dE_\gamma} = \frac{1}{2} \frac{r_\odot \rho_\odot^2 \langle\sigma v\rangle}{4\pi m_\chi^2} \frac{dN_\gamma}{dE_\gamma} \bar{J}(\Delta\Omega) \Delta\Omega, \quad (69)$$

with $\bar{J}(\Delta\Omega) \equiv (1/\Delta\Omega) \int_{\Delta\Omega} J(\psi) d\Omega$ and $\Delta\Omega = 2\pi(1 - \cos\psi)$ for the region around the galactic center. For example, we have $\bar{J}(\Delta\Omega) \Delta\Omega \approx 1$ for $\Delta\Omega = 10^{-3}$ and $\bar{J}(\Delta\Omega) \Delta\Omega \approx 0.1$ sr for $\Delta\Omega = 10^{-5}$ sr using the NFW dark matter profile [39].

The gamma-rays from the μ -favored model point of the NMSSM have two sources: one is related to the muons in the final state and the other one is related to the bottom quarks in the annihilation final state. Altogether, we have

$$\frac{dN_\gamma}{dE_\gamma} = \text{Br}(a_2 \rightarrow a_1 h_1) \frac{dN_\gamma^\mu(E_{a_1})}{dE_\gamma} + \text{Br}(a_2 \rightarrow a_1 h_1) \frac{dN_\gamma^b(E_{h_1})}{dE_\gamma} + \text{Br}(a_2 \rightarrow b\bar{b}) \frac{dN_\gamma^b(E_{a_2})}{dE_\gamma}. \quad (70)$$

There are two processes to generate gamma-rays associated with the muon final state. One is through final state radiation (FSR) and the other one is from the radiative muon decays into photons. For the final state radiation, we have

$$\frac{dN_{\gamma,FSR}^\mu(E_{a_1})}{dE_\gamma} = \frac{2}{E_{a_1}} \int_{\frac{E_\gamma}{E_{a_1}}}^{\frac{M_{a_1}-2m_\mu}{M_{a_1}-m_\mu}} dx \frac{1}{x} \frac{\alpha}{\pi} \left(\frac{1 + (1-x)^2}{x} \right) \left(\log \left(\frac{M_{a_1}^2(1-x)}{m_\mu^2} \right) - 1 \right). \quad (71)$$

For the radiative muon decays: $\mu^- \rightarrow e^- \nu_\mu \bar{\nu}_e \gamma$ and $\mu^+ \rightarrow e^+ \nu_e \bar{\nu}_\mu \gamma$, one has [40]

$$\frac{dN_{\gamma,RAD}^\mu(E_{a_1})}{dE_\gamma} = \frac{2}{E_{a_1}} \int_{\frac{E_\gamma}{E_{a_1}}}^1 dx \frac{2}{x} \int_{\frac{2x}{1+\beta}}^{\min(1, \frac{2x}{1-\beta})} dy \frac{1}{y} \mathcal{F}(y). \quad (72)$$

with $\beta = \sqrt{1 - 4m_\mu^2/m_\phi^2}$ and $\mathcal{F}(y)$ as the photon spectrum in the muon rest frame and given by

$$\begin{aligned} \mathcal{F}(y) = & \frac{\alpha}{3\pi} \frac{1-y}{y} \left((3 - 2y + 4y^2 - 2y^3) \log \frac{m_\mu^2}{m_e^2} - \frac{17}{2} + \frac{23y}{6} - \frac{101y^2}{12} + \frac{55y^3}{12} \right. \\ & \left. + (3 - 2y + 4y^2 - 2y^3) \log(1 - y) \right), \end{aligned} \quad (73)$$

with $y = 2E_\gamma/m_\mu$.

The gamma-ray fragmentation function from bottom quarks in the dark matter annihilation final state is simulated using PYTHIA and fitted using the following analytic function:

$$\frac{dN_\gamma^b(E)}{dE_\gamma} = \frac{2}{E} e^{7.59 - 80.25x + 412.5x^2 - 1297.7x^3 + 1969.7x^4 - 1137.8x^5}, \quad (74)$$

with $x \equiv 2E_\gamma/E$ and E as the center of mass energy of the $b\bar{b}$ system.

Summing up all contributions to the gamma-rays, we compare the model predictions with the background for gamma-ray energy above 1 GeV, which is fitted by a power-law in Ref. [41] as

$$\frac{d^2\Phi_\gamma^{\text{BG}}}{d\Omega dE_\gamma} = 6 \times 10^{-5} \left(\frac{E_\gamma}{1\text{GeV}} \right)^{-2.72} \text{cm}^{-2}\text{s}^{-1}\text{sr}^{-1}\text{GeV}^{-1}. \quad (75)$$

The Fermi LAT collaboration has already shown a preliminary result for the gamma rays from $0^\circ \leq l \leq 360^\circ$ and $10^\circ \leq |b| \leq 20^\circ$ [42]. Here, l and b are the heliocentric galactic coordinates. This region of angles corresponds to $\Delta\Omega = 0.567$ sr. It is easy to calculate $\bar{J}\Delta\Omega$ to be 13.4 for the NFW profile and 5.7 for the ISO profile. In Fig. 8, we show the observed gamma ray fluxes from Fermi LAT together with the data from EGRET. As one can see, there is a disagreement between those two experiments for photon energy above 1 GeV. The

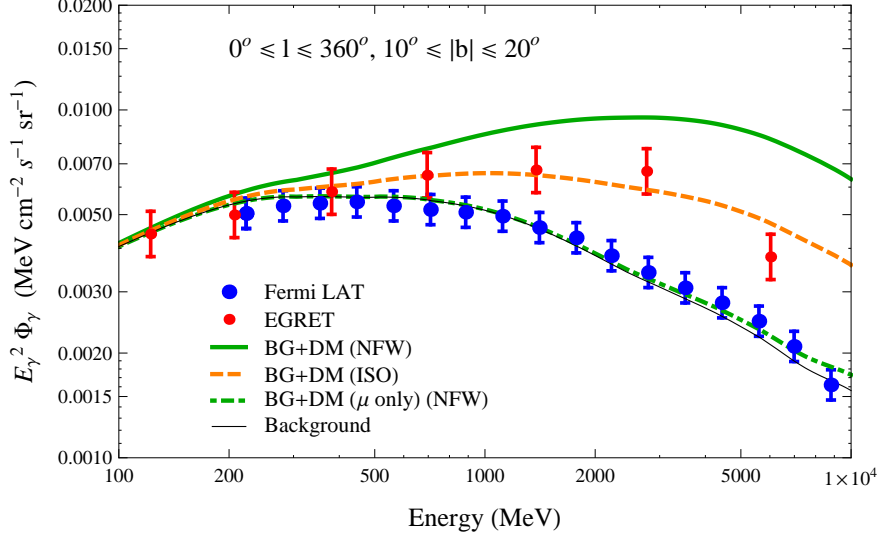


Figure 8: The gamma ray flux predicted from the neutralino annihilations in the NMSSM. The neutralino mass is $m_\chi = 162$ GeV and its annihilation cross section is $6.0 \times 10^{-24} \text{ cm}^2 \text{ s}^{-1}$. The solid green line is the dark matter prediction using the NFW profile plus the traditional background (shown as the thin black line). The dashed orange line is the dark matter prediction using the cored isothermal dark matter profile. The dot-dashed green line is the dark matter prediction without including the contributions from b quarks.

predictions from dark matter annihilation using the model point in Table 1 tend to agree with the EGRET result if one uses the ISO dark matter profile.

A larger discrepancy occurs for the dark matter prediction using the NFW profile. This might be reconciled by astrophysical uncertainties like the smoothness of the dark matter distribution, which affects the necessary dark matter annihilation cross section by a factor of a few. Notice also in Fig. 8 the dot-dashed green line showing the signal gamma-ray contribution from the muon final states only; this indicates that the discrepancy is coming from the b quarks in the final state.

We can also consider gamma rays coming from the galactic center. In Fig. 9, we compare the differential gamma-ray flux predicted from the neutralino annihilations in the NMSSM to the flux from the background, after fitting the positron fraction spectrum of PAMELA. We

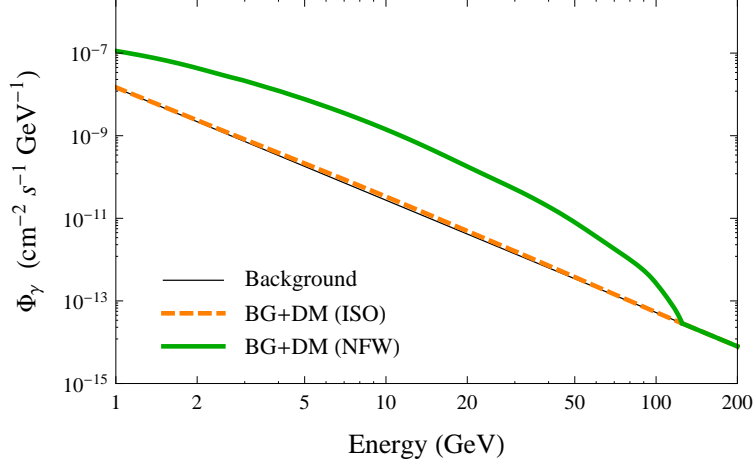


Figure 9: The photon flux predicted from the neutralino annihilations in the NMSSM after fitting the positron fraction spectrum of PAMELA. The neutralino mass is $m_\chi = 162$ GeV and its annihilation cross section is $6.0 \times 10^{-24} \text{ cm}^2 \text{ s}^{-1}$. $\Delta\Omega = 2.4 \times 10^{-4}$ ($0.5^\circ \times 0.5^\circ$ about the galactic center) and $\bar{J}\Delta\Omega \approx 0.69$ (NFW) and $\bar{J}\Delta\Omega \approx 0.003$ (ISO) are used here.

present the comparison of the model predictions and the background for a $0.5^\circ \times 0.5^\circ$ region about the galactic center. Since the Fermi LAT will have an angular resolution of around $0.1^\circ \times 0.1^\circ$ (10^{-5} sr), the error of their measurements in principle is small enough to test the dark matter annihilation scenario. However, the model predictions for the gamma-ray flux in the galactic center are subject to large uncertainties from the dark matter profile, which can bring a factor of few hundred difference as seen from Fig. 9.

Due to kinematical reasons, our dark matter neutralino mass is less than the top quark mass. Therefore, the gamma rays predicted in this model have an energy cutoff below the top quark mass. Hence, this model automatically evades the constraints from HESS, which measured the gamma-ray flux with energy above 200 GeV. For EGRET with $\Delta\Omega = 10^{-3}$ around the galactic center and with the energy range of $1 \text{ GeV} \leq E_\gamma \leq 30 \text{ GeV}$, the total background flux is $3 \times 10^{-8} \text{ cm}^{-2} \text{ s}^{-1}$. The dark matter contribution in this model is around $2 \times 10^{-7} \text{ cm}^{-2} \text{ s}^{-1}$ for the NFW profile and $1.5 \times 10^{-9} \text{ cm}^{-2} \text{ s}^{-1}$ for the ISO profile. This indicates a tension between the model prediction with the NFW profile and the EGRET

data. Again this result is subject to astrophysical uncertainties; for a solid angle around the galactic center, changing the dark matter profile can introduce an uncertainty of two orders of magnitude in the gamma-rays flux predictions.

7 Direct constraints

There are many direct constraints on the NMSSM parameter space from LEP, Tevatron, CLEO, B-factories and the magnetic moment of the muon. Our analysis shows that the most stringent constraints are from exclusive $\Upsilon(3S)$ decays at BaBar and light pseudoscalar searches at D0. Compared to the MSSM, the constraints from LEP and other searches are less severe, due to non-standard decays of the MSSM-like Higgs boson and a new suppression factor $\cos\theta_A$ beyond the MSSM.

7.1 LEP constraints

The heavier bosons in the NMSSM, typically above 250 GeV, were inaccessible at LEP. Therefore, we only consider the two lightest scalar particles a_1 and h_1 at LEP. There are three main production mechanisms for those two neutral Higgs bosons. One is through the Higgsstrahlung process $e^+e^- \rightarrow h_1 Z$; another one is the pair production process $e^+e^- \rightarrow h_1 a_1$; the third one is through the radiation off a massive fermion: $e^+e^- \rightarrow b\bar{b}a_1$.

For the Higgsstrahlung process $e^+e^- \rightarrow h_1 Z$ and for an h_1 mass within the LEP reach, the h_1 mainly decays to $b\bar{b}$ and $2a_1$ for the μ -favored and τ -favored cases, respectively. For the τ -favored model point, there are many different final states like 4τ , $2\tau 2g$ and so on. Although the LEP bounds on each of those channels are weak, the decay mode independent limits impose a bound on the mass of h_1 as $M_{h_1} > 82$ GeV [43], which is satisfied in the model points we have considered in this paper. For the μ -favored case, the lower bound on the h_1 mass is around 114 GeV, which is also satisfied for the model point reported in Table 1.

The cross section of the pair production process $e^+e^- \rightarrow h_1 a_1$ is proportional to $\cos^2\theta_A M_Z^4/M_{a_2}^4$ from Eq. (27), and hence is tiny for $\cos\theta_A < 0.3$ and $M_{a_2} > 300$ GeV. For

$\sqrt{s} = 200$ GeV, the cross section is calculated to be 2×10^{-3} fb for the model parameters in Table 1. Considering the integrated luminosity of LEP is below 1 fb^{-1} , there are no constraints on the model parameters from this channel.

Finally, for the associated production with bottom quarks, the cross section is also suppressed due to a moderate $\tan \beta$ and three-body final state phase space. The cross section for $e^+ e^- \rightarrow b \bar{b} a_1$ at $\sqrt{s} = 200$ GeV is calculated to be 1.5×10^{-3} fb for the model parameters in Table 1, which also indicates no constraints from LEP.

7.2 Tevatron constraints

The lightest CP -even Higgs boson h_1 has approximately the same couplings to fermions as in the Standard Model. The ongoing searches at CDF and D0 do not yet constrain an h_1 with a mass around 115 GeV at the Tevatron [44].

For the lightest CP -odd Higgs boson a_1 , the main production process at the Tevatron is through associated production with $b \bar{b}$ and has a cross section proportional to $\tan^2 \beta \cos^2 \theta_A \sigma(b \bar{b} \phi_{\text{SM}})$, where ϕ has the same coupling to $b \bar{b}$ as the SM Higgs boson. Although the production cross section can be large for the model parameters that we consider, the existing searches at D0 for the a_1 decays to two taus only constrain an a_1 with a mass above 90 GeV [45].

However, the recent searches for a_1 in the channel $h_1 \rightarrow a_1 a_1 \rightarrow \mu^+ \mu^- \mu^+ \mu^-$ at D0 can impose a stringent bound on the muon-favored model parameter space in the NMSSM. The SM background for two pairs of collinear muons is very small (below 0.02 events for 3.7 fb^{-1} integrated luminosity), and the null result imposes a constraint $\sigma(p \bar{p} \rightarrow h_1 + X) \cdot \text{Br}(h_1 \rightarrow a_1 a_1) \cdot \text{Br}(a_1 \rightarrow \mu^+ \mu^-)^2 \lesssim 10 \text{ fb}$ [46]. This bound is roughly independent of the a_1 mass. The production cross section for a SM Higgs at the Tevatron is around 0.8 pb, so we need to have $\text{Br}(h_1 \rightarrow a_1 a_1) \lesssim 1.2\%$ for $\text{Br}(a_1 \rightarrow \mu^+ \mu^-) \approx 100\%$. Therefore, the muon-favored model point in Table 1 is allowed by this constraint, although it selects a specific region of the NMSSM parameter space. This experimental result points to small values of λ and κ to decrease the h_1 branching ratio into $a_1 a_1$. However, small values of λ and κ also increase the branching ratio of a_2 into $b \bar{b}$. Since the dominant annihilation is mediated by

the resonance effect with a_2 , this leads to a non-negligible hadronic final state from the dark matter annihilation.

7.3 The magnetic moment of the muon

There is a new radiative contribution to the magnetic moment of the muon by exchanging a_1 in the loop diagram. Using the one-loop result from Ref. [47], the new physics correction to a_μ is

$$\delta a_\mu = \frac{g_2^2 m_\mu^2}{32 \pi^2 M_W^2} (\cos \theta_A \tan \beta)^2 \times \frac{m_\mu^2}{M_{a_1}^2} \int_0^1 \frac{-x^3 dx}{x^2(m_\mu^2/M_{a_1}^2) + 1 - x}, \quad (76)$$

and is negative. The two-loop calculation will not change the sign of δa_μ for a mass of a_1 below 1 GeV [14]. The measured value of a_μ has a 3.4σ deviation ($e^+ e^-$ data only) above the prediction of the standard model [48]. Requiring the new physics to be less than the experimental error, we arrive at the following constraints on the model parameters:

$$\cos \theta_A \tan \beta \lesssim 2.5 \quad (\text{BNL } (g-2)_\mu/2). \quad (77)$$

Here M_{a_1} is chosen to be 800 MeV, while the constraints are less stringent as one increases M_{a_1} .

Notice that the δa_μ may also receive significant contributions from other particles like smuons, that we chose to be heavy here to isolate the dark matter discussions.

7.4 Constraints from Upsilon decays

Another stringent bound on the NMSSM parameter space with a light a_1 below 10 GeV is from Upsilon decays into a photon plus a_1 , which decays into a pair of taus or muons.

For the mass range $2m_\tau < m_{a_1} < 9.2$ GeV, the strongest bound is from the recent CLEO-III limits [49] on $\Upsilon(1S) \rightarrow \gamma \tau^+ \tau^-$. The radiative decay to $\Upsilon(1S) \rightarrow \gamma a_1$ is calculated as [50]

$$\frac{\mathcal{B}(\Upsilon(1S) \rightarrow \gamma a_1)}{\mathcal{B}(\Upsilon(1S) \rightarrow \mu^+ \mu^-)} = \frac{G_F m_b^2}{\sqrt{2} \pi \alpha} (\cos \theta_A \tan \beta)^2 \left(1 - \frac{M_{a_1}^2}{M_{\Upsilon(1S)}^2} \right) \mathcal{F}, \quad (78)$$

where $\mathcal{F} \sim 0.5$ incorporates QCD and relativistic corrections [51] [52]. The data from CLEO have the limit $\mathcal{B}(\Upsilon(1S) \rightarrow \gamma a_1) \times \mathcal{B}(a_1 \rightarrow \tau^+ \tau^-) \lesssim 5 \times 10^{-5}$ at 90% C.L. for a wide range of M_{a_1} between 4 GeV to 9 GeV. Using $\mathcal{B}(\Upsilon(1S) \rightarrow \mu^+ \mu^-) = 2.48\%$ and $\mathcal{B}(a_1 \rightarrow \tau^+ \tau^-) \approx 0.9$ from the model prediction, this limit is translated into a bound on $\cos \theta_A \tan \beta$ as

$$\cos \theta_A \tan \beta \lesssim 0.9 \quad (\text{CLEO} - \text{III}). \quad (79)$$

For the mass range $2m_\mu < m_{a_1} < 1 \text{ GeV}$, the strongest current bound is coming from the light scalar searches in the channel $\Upsilon(3S) \rightarrow \gamma a_1$ at BaBar. At 90% C.L., BaBar imposes an upper limit $\mathcal{B}(\Upsilon(3S) \rightarrow \gamma a_1) \times \mathcal{B}(a_1 \rightarrow \mu^+ \mu^-) \lesssim 5.2 \times 10^{-6}$ [53] for M_{a_1} below 1 GeV. Using $\mathcal{B}(\Upsilon(3S) \rightarrow \mu^+ \mu^-) = 2.18\%$ and $\mathcal{B}(a_1 \rightarrow \mu^+ \mu^-) \approx 1.0$ from the model prediction, this limit is translated into a bound on $\cos \theta_A \tan \beta$ as

$$\cos \theta_A \tan \beta \lesssim 0.4 \quad (\text{BaBar}). \quad (80)$$

For the range of $2m_\mu < m_{a_1} < M_K - M_\pi$, the decay mode $K^+ \rightarrow \pi^+ a_1$ is open. The branching ratio of this decay channel is given by [54]

$$\begin{aligned} \mathcal{B}(K^+ \rightarrow \pi^+ a_1) &= \frac{G_F f_\pi^2}{\sqrt{2}} (\tan \beta - \tan^{-1} \beta)^2 \cos^2 \theta_A \frac{\Gamma(K_s^0 \rightarrow \pi^0 \pi^0)}{\Gamma(K^+ \rightarrow \text{all})} \\ &= 3 \times 10^{-6} (\tan \beta - \tan^{-1} \beta)^2 \cos^2 \theta_A, \end{aligned} \quad (81)$$

which should be compared to the experimental values from the HyperCP collaboration [55]: $\mathcal{B}(K^+ \rightarrow \pi^+ \mu^+ \mu^-) = 9.8 \pm 1.0 \pm 0.5 \times 10^{-8}$. Therefore, the following constraint on the model parameter space is derived

$$\cos \theta_A |\tan \beta - \tan^{-1} \beta| \lesssim 0.06 \quad (\text{HyperCP}), \quad (82)$$

So, other than when $\tan \beta$ is very close to 1 or $\cos \theta_A$ is extremely close to zero, the mass of a_1 is constrained to be above $M_K - M_\pi \sim 360 \text{ MeV}$.

Finally, there are also other constraints from B-physics like $b \rightarrow s \gamma$ or $B_s \rightarrow \mu^+ \mu^-$. Since the a_1 pseudoscalar does not mediate tree-level flavor-changing processes, one can use

the minimal flavor violation assumption to suppress many kinds of flavor changing processes. We have used the NMHDECAY program to check those constraints and to justify the validity of our model points. In short, the most stringent constraint for $M_K - M_\pi < m_{a_1} < 1$ GeV is the radiative decays of Upsilon into photons from BaBar. The bound is $\cos \theta_A \tan \beta \lesssim 0.4$. One can see that the model point in Table 1 satisfies this bound.

8 Discussions and Conclusions

The dark matter candidate neutralino in the NMSSM from Table 1 is a combination of the bino, wino and Higgsino. Therefore, it has a good chance to be detected in dark matter direct detection experiments, especially from the spin-dependent elastic scattering with nucleons. Here we just report the values calculated using the micrOMEGAs program [56]. The spin-independent DM-proton and DM-neutron cross sections are $0.7 \times 10^{-45} \text{ cm}^2$ and $0.9 \times 10^{-45} \text{ cm}^2$, which are two orders of magnitude below the current bounds from XENON10 [57]. For the spin-dependent one, the DM-proton and DM-neutron cross sections are $1.5 \times 10^{-39} \text{ cm}^2$ and $1.2 \times 10^{-39} \text{ cm}^2$. The later one is only one order of magnitude below the current bound [58] and is in the accessible region of the upgraded experiments.

The NMSSM explanation of the PAMELA positron excess can be tested by future experiments at colliders and new results from cosmic ray experiments. On the collider side, it is important to measure the masses of the neutralino and the heavier CP -odd particle. If their masses satisfy the relation $M_{a_2} \approx 2m_\chi$, the large dark matter annihilation cross section can be confirmed. Another important quantity to measure is the mass of the lighter CP -odd particle, because the PAMELA positron excess prefers to have its mass below 1 GeV. It is also crucial to know the branching ratio of a_2 to $b\bar{b}$, since the dominant antiproton contributions are from this channel.

On the cosmic ray side, we make a well-motivated unambiguous prediction that PAMELA will observe a turnover of the rising positron spectrum at around 70 GeV. The additional contributions to the electron+positron spectrum from dark matter annihilations are within current uncertainties but could be resolved in the future by Fermi LAT. The associated

gamma-ray flux from dark matter annihilation could also be resolved by Fermi LAT, but again due to astrophysical uncertainties one should be cautious when making a concrete prediction.

In this paper we have explored the possibility of using neutralino annihilations in the NMSSM to explain the positron excess observed at PAMELA. Kinematics plays an essential role for having a viable model with a large fraction of leptons and a small fraction of hadrons in the annihilation final state. The lighter CP -odd particle a_1 has a mass below 1 GeV and mainly decays into two muons. The dark matter neutralino mass is less than the top quark mass to forbid the otherwise dominant $t\bar{t}$ final state. The s -channel resonance effect with the heavier CP -odd particle a_2 increases the dark matter annihilation cross section to match the necessary one for the PAMELA positron fraction spectrum; this also requires that the neutralino mass is less than the top quark mass, to avoid smearing the resonance effect from a large $t\bar{t}$ contribution to the a_2 width.

An NMSSM explanation of PAMELA makes three striking and uniquely correlated predictions: the rise in the PAMELA positron spectrum will turn over at around 70 GeV, the dark matter particle mass is less than the top quark mass, and a light sub-GeV pseudoscalar will be discovered at colliders.

Acknowledgments: The authors are grateful to Laura Covi, Gordon Kane, Maurizio Pierini and Peter Skands for useful discussions. Fermilab is operated by Fermi Research Alliance, LLC under contract no. DE-AC02-07CH11359 with the United States Department of Energy.

References

- [1] O. Adriani *et al.* [PAMELA Collaboration], *Nature* **458**, 607 (2009) [arXiv:0810.4995].
- [2] O. Adriani *et al.*, *Phys. Rev. Lett.* **102**, 051101 (2009) [arXiv:0810.4994].

- [3] M. Cirelli and A. Strumia, arXiv:0808.3867; V. Barger, W. Y. Keung, D. Marfatia and G. Shaughnessy, Phys. Lett. B **672**, 141 (2009) [arXiv:0809.0162]; I. Cholis, L. Goode-nough, D. Hooper, M. Simet and N. Weiner, arXiv:0809.1683.
- [4] M. Cirelli, M. Kadastik, M. Raidal and A. Strumia, Nucl. Phys. B **813**, 1 (2009) [arXiv:0809.2409].
- [5] N. Arkani-Hamed, D. P. Finkbeiner, T. R. Slatyer and N. Weiner, Phys. Rev. D **79**, 015014 (2009) [arXiv:0810.0713].
- [6] Y. Bai and Z. Han, arXiv:0811.0387; P. J. Fox and E. Poppitz, arXiv:0811.0399.
- [7] J. Hisano, S. Matsumoto and M. M. Nojiri, Phys. Rev. Lett. **92**, 031303 (2004).
- [8] N. Arkani-Hamed and N. Weiner, JHEP **0812**, 104 (2008) [arXiv:0810.0714].
- [9] Y. Bai and Z. Han, arXiv:0902.0006.
- [10] T. Moroi and L. Randall, Nucl. Phys. B **570**, 455 (2000) [arXiv:hep-ph/9906527]; B. S. Acharya, P. Kumar, K. Bobkov, G. Kane, J. Shao and S. Watson, JHEP **0806**, 064 (2008) [arXiv:0804.0863]; M. Pospelov and M. Trott, JHEP **0904**, 044 (2009) [arXiv:0812.0432].
- [11] P. Grajek, G. Kane, D. Phalen, A. Pierce and S. Watson, arXiv:0812.4555.
- [12] J. R. Ellis, J. F. Gunion, H. E. Haber, L. Roszkowski and F. Zwirner, Phys. Rev. D **39**, 844 (1989).
- [13] R. Dermisek and J. F. Gunion, Phys. Rev. Lett. **95**, 041801 (2005) [arXiv:hep-ph/0502105]; R. Dermisek and J. F. Gunion, Phys. Rev. D **73**, 111701 (2006) [arXiv:hep-ph/0510322]; R. Dermisek and J. F. Gunion, Phys. Rev. D **79**, 055014 (2009) [arXiv:0811.3537].
- [14] J. F. Gunion, D. Hooper and B. McElrath, Phys. Rev. D **73**, 015011 (2006) [arXiv:hep-ph/0509024].

- [15] U. Ellwanger, J. F. Gunion and C. Hugonie, JHEP **0502**, 066 (2005) [arXiv:hep-ph/0406215].
- [16] C. Panagiotakopoulos and K. Tamvakis, Phys. Lett. B **446**, 224 (1999) [arXiv:hep-ph/9809475].
- [17] R. Dermisek and J. F. Gunion, Phys. Rev. D **75**, 075019 (2007) [arXiv:hep-ph/0611142].
- [18] F. Bergsma *et al.* [CHARM Collaboration], Phys. Lett. B **157**, 458 (1985).
- [19] The CDF collaboration, http://www-cdf.fnal.gov/physics/new/top/public_mass.html.
- [20] Y. Nomura and J. Thaler, arXiv:0810.5397.
- [21] J. F. Navarro, C. S. Frenk and S. D. M. White, Astrophys. J. **490**, 493 (1997) [arXiv:astro-ph/9611107].
- [22] J. N. Bahcall and R. M. Soneira, Astrophys. J. Suppl. **44**, 73 (1980).
- [23] T. Sjostrand, S. Mrenna and P. Skands, JHEP **0605**, 026 (2006) [arXiv:hep-ph/0603175].
- [24] S. Jadach, Z. Was, R. Decker and J. H. Kuhn, Comput. Phys. Commun. **76**, 361 (1993).
- [25] T. Delahaye, R. Lineros, F. Donato, N. Fornengo and P. Salati, Phys. Rev. D **77**, 063527 (2008) [arXiv:0712.2312].
- [26] F. Donato, D. Maurin, P. Salati, A. Barrau, G. Boudoul and R. Taillet, Astrophys. J. **563**, 172 (2001) [arXiv:astro-ph/0103150]; F. Donato, N. Fornengo, D. Maurin and P. Salati, Phys. Rev. D **69**, 063501 (2004) [arXiv:astro-ph/0306207].
- [27] M. Cirelli, R. Franceschini and A. Strumia, Nucl. Phys. B **800**, 204 (2008) [arXiv:0802.3378].
- [28] J. Clem, *et. cl.* Astrophys. J. **464**, 507 (1998).

- [29] I. V. Moskalenko and A. W. Strong, *Astrophys. J.* **493**, 694 (1998) [arXiv:astro-ph/9710124].
- [30] E. A. Baltz and J. Edsjo, *Phys. Rev. D* **59**, 023511 (1999) [arXiv:astro-ph/9808243].
- [31] Fermi LAT Collaboration, arXiv:0905.0025 [astro-ph.HE].
- [32] L. C. Tan and L. K. Ng, *J. Phys. G* **9**, 227 (1983).
- [33] R. J. Protheroe, *Astrophys. J.* **251**, 387 (1981).
- [34] J. Alcaraz *et al.* [AMS Collaboration], *Phys. Lett. B* **490**, 27 (2000).
- [35] M. Boezio *et al.*, *Astropart. Phys.* **19**, 583 (2003) [arXiv:astro-ph/0212253].
- [36] T. Bringmann and P. Salati, *Phys. Rev. D* **75**, 083006 (2007) [arXiv:astro-ph/0612514].
- [37] F. Aharonian *et al.* [H.E.S.S. Collaboration], *Phys. Rev. Lett.* **101**, 261104 (2008) [arXiv:0811.3894].
- [38] S. D. Hunter *et al.*, *Astrophys. J.* **481** (1997) 205.
- [39] E. Ponton and L. Randall, *JHEP* **0904**, 080 (2009) [arXiv:0811.1029].
- [40] R. Essig, N. Sehgal and L. E. Strigari, arXiv:0902.4750 and references therein.
- [41] L. Bergstrom, P. Ullio and J. H. Buckley, *Astropart. Phys.* **9**, 137 (1998) [arXiv:astro-ph/9712318].
- [42] N. Giglietto, on behalf of the FERMI LAT collaboration, at La Thuile 2009.
- [43] G. Abbiendi *et al.* [OPAL Collaboration], *Eur. Phys. J. C* **27**, 311 (2003) [arXiv:hep-ex/0206022].
- [44] T. N. Phenomena, H. w. group, f. t. C. collaboration and D. collaboration, arXiv:0903.4001.

- [45] V. M. Abazov *et al.* [D0 Collaboration], Phys. Rev. Lett. **102**, 051804 (2009) [arXiv:0811.0024].
- [46] The D0 collaboration, D0Note 5891-CONF.
- [47] M. Krawczyk, arXiv:hep-ph/0103223.
- [48] G. W. Bennett *et al.* [Muon G-2 Collaboration], Phys. Rev. D **73**, 072003 (2006) [arXiv:hep-ex/0602035]; M. Passera, W. J. Marciano and A. Sirlin, AIP Conf. Proc. **1078**, 378 (2009) [arXiv:0809.4062].
- [49] W. Love *et al.* [CLEO Collaboration], Phys. Rev. Lett. **101**, 151802 (2008) [arXiv:0807.1427].
- [50] F. Wilczek, Phys. Rev. Lett. **39**, 1304 (1977).
- [51] M. L. Mangano and P. Nason, Mod. Phys. Lett. A **22**, 1373 (2007) [arXiv:0704.1719].
- [52] I. G. Aznaurian, S. G. Grigorian and S. G. Matinyan, JETP Lett. **43**, 646 (1986).
- [53] B. Aubert [The BABAR Collaboration], arXiv:0902.2176.
- [54] W. A. Bardeen, S. H. Tye and J. A. M. Vermaseren, Phys. Lett. B **76**, 580 (1978).
- [55] H. K. Park *et al.* [HyperCP Collaboration], Phys. Rev. Lett. **88**, 111801 (2002) [arXiv:hep-ex/0110033].
- [56] G. Belanger, F. Boudjema, A. Pukhov and A. Semenov, arXiv:0803.2360.
- [57] J. Angle *et al.* [XENON Collaboration], Phys. Rev. Lett. **100**, 021303 (2008) [arXiv:0706.0039].
- [58] J. Angle *et al.*, Phys. Rev. Lett. **101**, 091301 (2008) [arXiv:0805.2939].